COMPUTATIONAL MODELLING OF GEOMETRIC AND MATERIAL NONLINEARITIES AND THEIR EFFECTS ON FRACTURE PARAMETERS

by

N. Meherphani Lalith Kumar

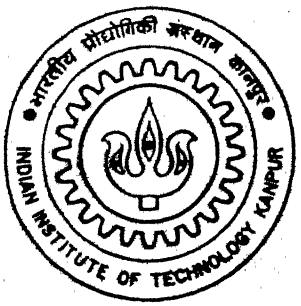

DEPARTMENT OF MECHANICAL ENGINEERING

INDIAN INSTITUTE OF TECHNOLOGY KANPUR

JANUARY, 1995

COMPUTATIONAL MODELLING OF GEOMETRIC AND MATERIAL NONLINEARITIES AND THEIR EFFECTS ON FRACTURE PARAMETERS

A Thesis Submitted
in Partial Fulfilment of the Requirements
for the Degree of

MASTER of TECHNOLOGY

by

N. Meherphani Lalith Kumar

to the

DEPARTMENT OF MECHANICAL ENGINEERING
INDIAN INSTITUTE OF TECHNOLOGY KANPUR
KANPUR

JANUARY, 1995

CERTIFICATE

This is to certify that the work contained in this thesis entitled **Computational Modelling of Geometric and Material Nonlinearities and their effects on Fracture Parameters** by **N.Meherphani Lalith Kumar** has been carried out under my supervision and that this work has not been submitted elsewhere for a degree.

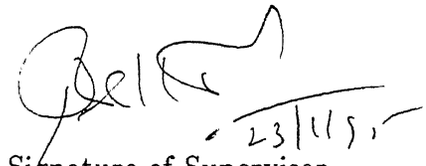

Signature of Supervisor
Name : Dr. Raju Sethuraman
Assistant Professor
Department of Mechanical Engineering
Indian Institute of Technology Kanpur
Kanpur, INDIA

January, 1995

ACKNOWLEDGEMENTS

I wish to express my deep sense of gratitude and sincere thanks to my thesis supervisor Dr. Raju Sethuraman for his inspiring guidance and constant encouragement throughout this work. It was a rewarding experience to work under him.

Words cannot express my feelings towards my wife for her Patience and Cooperation.

To the memory of
My Beloved Mother

Abstract

Geometric and Material Nonlinearities which arise due to large deformations are modelled in the present work using finite element method. Modelling of large deformations is based on Total Lagrangian formulation. Materials having elastic-perfectly plastic and elastic-linearly work hardening characteristics are considered in the present study. Fracture parameters, Energy Release Rate and Crack Tip Opening Displacement (CTOD) are evaluated for a simply supported beam with central crack and a plate with center and edge crack of finite dimensions.

List of Figures

List of Tables

NOMENCLATURE

${}^{t+\Delta t}\tau_{ij}$	=	Components of Cauchy stress tensor at time t+ Δt
${}^{t+\Delta t}e_{ij}$	=	Components of infinetesimal strain tensor at time t+Δt
${}^{t+\Delta t}V$	=	Volume of the body at time t+Δt
u_i	=	Increment in displacement component
${}^{t+\Delta t}A$	=	Area of the body at time t+Δt
${}^{t+\Delta t}t_i$	=	Components of externally applied body force vectors at time t+Δt
${}^{t+\Delta t}f_i$	=	Components of externally applied surface force vectors at time t+Δt
${}^{t}_{0}S_{ij}$	=	Second Piola-Kirchhoff stress at time t referred to time 0
${}^{t}_{0}\epsilon_{ij}$	=	Green-Lagrange Strain at time t referred to time 0
${}^{t+\Delta t}R$	=	External work at time t+Δt
${}^{0}\rho$	=	Specific mass of the body at time 0
${}^{0}x_i$	=	Cartesian coordinates at time 0
${}_{0}S_{ij}$	=	Component of Second Piola-Kirchhoff stress increment at time 0
${}_{0}\epsilon_{ij}$	=	Component of Green-Lagrange strain increment at time 0
${}_{0}e_{ij}$, ${}_{0}\eta_{ij}$	=	Linear and Non-linear part of strain increment in ${}_{0}\epsilon_{ij}$
${}_{0}C_{ijrs}$	=	Incremental material property tensor
${}^{t}_{0}C_{ijrs}$	=	Material property tensor at time t referred to configuration at time 0
h_k	=	Finite element interpolation function associated with nodal point k
${}^{t}u^{k}_{i}$	=	Displacement component of nodal point k at time t
Δu^{k}_{i}	=	Increment in u^{k}_{i}
$\sigma_x, \sigma_y, \sigma_z$	=	Normal stresses in x,y and z directions respectively
$\tau_{xy}, \tau_{yz}, \tau_{zx}$	=	Shear stresses
$d\epsilon_{ij}$	=	Incremental strain tensor

$(d\epsilon_{ij})_e$	=	Incremental elastic strain tensor
$(d\epsilon_{ij})_p$	=	Incremental plastic strain tensor
$d\sigma'_{ij}$	=	Incremental deviatoric stress components
$d\sigma_{kk}$	=	Incremental hydrostatic stress components
$f(\sigma)$	=	Yield function
H'	=	Strain hardening parameter
W	=	Strain energy density
V	=	Potential energy
J_1, J_2, J_3	=	Stress invariants
Q	=	Plastic potential
$\overline{\sigma}$	=	Equivalent stress
D	=	Matrix of elastic constants
D_{ep}	=	Elasto-plastic material matrix
${}^t_0B_L$	=	Linear strain displacement matrix at time t referred to time 0
${}^t_0B_{NL}$	=	Non-linear strain displacement matrix at time t referred to time 0
${}^t_0K_L$, ${}^t_0K_{NL}$	=	Linear and Non-linear stiffness matrices at time t referred to time 0
${}^t_0F$	=	Vector of nodal point forces equivalent to the element stresses at time t referred to time 0
${}^{t+\Delta t}R$	=	Vector of externally applied nodal point loads at time t+Δt
${}^t_0S$	=	Second Piola-Kirchhoff stress matrix at time t referred to time 0
${}^t_0\tilde{S}$	=	Second Piola-Kirchhoff Stress tensor at time t referred to time 0
${}_0C$	=	Material property matrix

Contents

Chapter 1

INTRODUCTION

1.1 Importance of the Problem

Fracture mechanics supposes the pre-existence of a significant crack like defect that will lead to failure. Elastic or elastic plastic continuum mechanics theory is used to develop parameters which characterise the crack tip stress field. If a material property is measured in terms of suitable parameters under known circumstances, fracture mechanics then allows this property to be used to calculate the behavior of other geometrical configurations for similar physical circumstances.

When a body having cracks is subjected to loading there will be large deformation and also a plastic zone in front of the crack tip. Much work has been done in recent years to estimate the fracture parameter of interest in cracked bodies. However, most of the earlier analyses were based on linear elastic behavior and assume the deformations to be small. Some work was also carried out to study the effect of large deformations on fracture parameters. However, most of this was limited to Linear Elastic Fracture Mechanics (LEFM).

Unfortunately, in many engineering problems it is indispensable to consider the effects of geometric and material nonlinearities. In metal-forming processes, work-pieces may undergo quite large displacements, large rotations, and large deformation. In addition when the stress or strain within the material reaches a certain level, the deformation of the material will no longer be linearly elastic, and non-linearly elastic or plastic deformation will occur. with plastic deformation, the stress-strain relation is no longer unique and will depend on deformation history. In fact, even when the global deformation of a structure can be regarded as elastic, local plastic deformation can often be found in the structure. This is especially true when contacts or cracks are present, since contacts can often produce high local pressures on contacting boundaries and there will be a plastic zone ahead of the crack tip. More importantly, many contact-impact problems of great interest involve plastic deforma-

tion. In metal-forming processes, for example, plastic deformation of the work piece is involved without exception. Another important case in which plastic deformation is involved is structural crashworthiness analysis in which structures are often subjected to heavy loadings.

Thus, it can be concluded that it is very important to model large elastic-plastic deformations in engineering problems. The present work is aimed at modelling large elastic-plastic deformations and estimating the effect of geometric nonlinearity on fracture parameters for two dimensional bodies under plane stress/plane strain conditions.

1.2 Literature Survey

Lagrangian formulation is by far the most widely used formulation in finite element applications to nonlinear structural problems [1-6]. Many of the early incremental formulations are incomplete in that the variations in loading and rotations of the element are not properly represented [5]. The most general approach to incremental lagrangian formulation is to consider a fully nonlinear kinematic relations within a linear increment [5,6].

When fully nonlinear kinematic relations are used within a linear increment, the number of stiffness contributions to the nonlinear element stiffness matrix are found to be three matrices [5,6]. These are the usual small displacement or the incremental stiffness matrix, the initial stress or the geometric or the tangent stiffness matrix and, finally the initial displacement or the initial rotation stiffness matrix.

Geometric nonlinearities were first included by means of incremental geometric stiffness [7-9]. Later two different approaches were pursued in incremental nonlinear finite element analysis. In the first approach referred to as the moving coordinate formulation, the static and kinematic variables were referred to the deformed configuration in each load step [11,12]. [13] gives some results based on this approach.

In the second approach, termed as the lagrangian formulation, the static and kinematic variables were referred to the initial configuration of the body. [5,6] used this approach.

Bathe et al [15] presented a more general finite element formulation based on continuum mechanics principles accounting for all nonlinearities and showed that the finite element solution based on the updated and total lagrangian configurations remained the same, provided proper constitutive relations are employed. It is the numerical effectiveness which governs the choice between the total and updated la-

grangian configurations.

In the study of fracture mechanics interest is often focussed on the singularity point where such quantities as stress become mathematically infinite. Crack tip elements were designed to simulate the singularity at the crack tip. [16-19] studied the use of crack tip elements in fracture problems. It was reported that the crack tip singularity characteristic of LEFM can be obtained in a 2D 8-noded isoparametric elements by shifting mid side nodes to the quarter point. The use of finite elements in fracture mechanics increased. But, many of the results were based on LEFM and do not consider the nonlinearities present in the structure.

[20] determined the combined effect of shear and large deformation on stress intensity factors. The influence of geometric nonlinearity on fracture parameter was found to be considerable. However, the study was still limited to LEFM.

In Elastic Plastic Fracture Mechanics(EPFM) J-Integral and CTOD are the generally used fracture parameters. [21] finds the J-criteria to be most attractive from computational viewpoint. [22] discusses the approaches to establish fracture criteria which would allow the engineer to decide whether a structure is safe against steady or unsteady crack growth under given conditions. [23] shows that calculation results obtained with the method of finite elements, employing an incremental plasticity model can serve to evaluate the independence of J. Crack tip opening displacement was also favored by some researchers. [24] studies the effect of thickness on crack opening displacement. [25] carries out fractographic studies of crack tips in steel and aluminium alloys.

[26] describes how triangular quarter point elements can be used as elastic as well as perfectly plastic crack tip elements. The elastic singularity $(1/\sqrt{r})$ is obtained by having one node at the crack tip. The plastic singularity $(1/r)$ is obtained by having multiple independent nodes at the crack tip. Geometric Nonlinearity is modelled using UL formulation in [35].

1.3 Outline of the Thesis

Importance of the problem and literature survey are discussed in chapter 1. Chapter 2 summarises the formulation of the general incremental equations of motion starting from continuum mechanics principle. The methodology for elastic-plastic analysis is explained. The total lagrangian formulation on which the present work is based is also discussed in detail in this chapter. Finite element implementation is discussed in chapter 3. Crack tip singularity modelling and evaluation of fracture parameters

is explained in chapter 4. Comparison of our results with available analytical results is given in chapter 5. Some more sample problems are also solved in this chapter. Chapter 6 gives conclusions and scope for further improvement in the present work.

Chapter 2

FORMULATION OF THE PROBLEM

The objective of this chapter is to give a continuum mechanics based incremental equations of motion which form the basis for general nonlinear finite element analysis. The equations of motion are based on the principle of virtual work which is dealt with in Section 2.1.1. The stress and strain tensors which are found to be appropriate in the incremental formulation of the virtual work principle are introduced in section 2.1.2. Section 2.1.3. deals with total lagrangian formulation which is widely used in large deformation analysis. The methodology for elastic-plastic analysis is given in section 2.1.4.

2.1 Formulation of the Continuum Mechanics Incremental Equations of Motion

In the conventional linear analysis of a body, the deformation of the body is assumed to be small, which means, the equations of motion for any applied load can be set up in the initial configuration of the body. But, in the more general analysis involving finite deformations, the equilibrium of the body has to be established in the current configuration. Unfortunately, the current configuration is what is the unknown quantity. This calls for the incremental analysis to be performed in the case of large deformation problems. These sections in this chapter aim at deriving the incremental equations of motion based on the virtual work principle.

2.1.1 Principle of Virtual Work

Consider the motion of a body in a cartesian coordinate system as shown in Fig. 2.1. It is assumed that the body can experience large displacements, small strains, large rotations and a nonlinear constitutive response. The aim is to evaluate the equilibrium states of the body at discrete times 0, Δt, $2\Delta t$, $3\Delta t$, where Δt is an increment in time.

The equilibrium of the body at time $t + \Delta t$ based on the principle of virtual displacements is given by

$$\int_{t+\Delta t V} {}^{t+\Delta t}\tau_{ij} \;\; \delta_{t+\Delta t}e_{ij} \;\; {}^{t+\Delta t}dV = {}^{t+\Delta t}R \tag{2.1}$$

In the above equation and the equations to follow, the left hand superscript denotes the configuration at which the quantity is measured and the left hand subscript denotes the configuration which is taken as reference for measurement. In case the quantity considered occurs in the same configuration in which it is measured, the left subscript is not used. Thus, ${}^{t+\Delta t}\tau_{ij}$ are the cartesian components of the cauchy stress tensor at $t+\Delta t$ and ${}_{t+\Delta t}e_{ij}$ are the cartesian components of infinitesimal strain tensor due to the virtual displacements δu and δ means "variation in" i.e.,

$$\delta_{t+\Delta t}e_{ij} = \delta\frac{1}{2}\left(\frac{\partial u_i}{\partial {}^{t+\Delta t}x_j} + \frac{\partial u_j}{\partial {}^{t+\Delta t}x_i}\right) = \frac{1}{2}\left(\frac{\partial \delta u_i}{\partial {}^{t+\Delta t}x_j} + \frac{\partial \delta u_j}{\partial {}^{t+\Delta t}x_i}\right)$$

It should be noted that the cauchy stresses are "body internal forces per unit area" in the configuration at time $t + \Delta t$ and the infinitesimal strain components are also referred to the equilibrium configuration at time $t + \Delta t$. L.H.S. of virtual work expression (2.1) is the internal virtual work performed when the body is subjected to virtual displacements at time $t + \Delta t$ and the corresponding external work due to virtual displacements is given by

$${}^{t+\Delta t}R = \int_{t+\Delta t A} {}^{t+\Delta t}f_i \;\; \delta u_i \;\; {}^{t+\Delta t}dA \;\; + \;\; \int_{t+\Delta t V} {}^{t+\Delta t}t_i \;\; \delta u_i \;\; {}^{t+\Delta t}dV \tag{2.2}$$

where ${}^{t+\Delta t}t_i$ and ${}^{t+\Delta t}f_i$ are the components of externally applied body and surface force vectors at time $t+\Delta t$ with reference to the same configuration. It is to be noted that the summation convention of tensor notation is followed throughout.

The difficulty in solving equation (2.1) is that the configuration at time $t + \Delta t$ is not known. This is an important difference compared with the linear analysis where

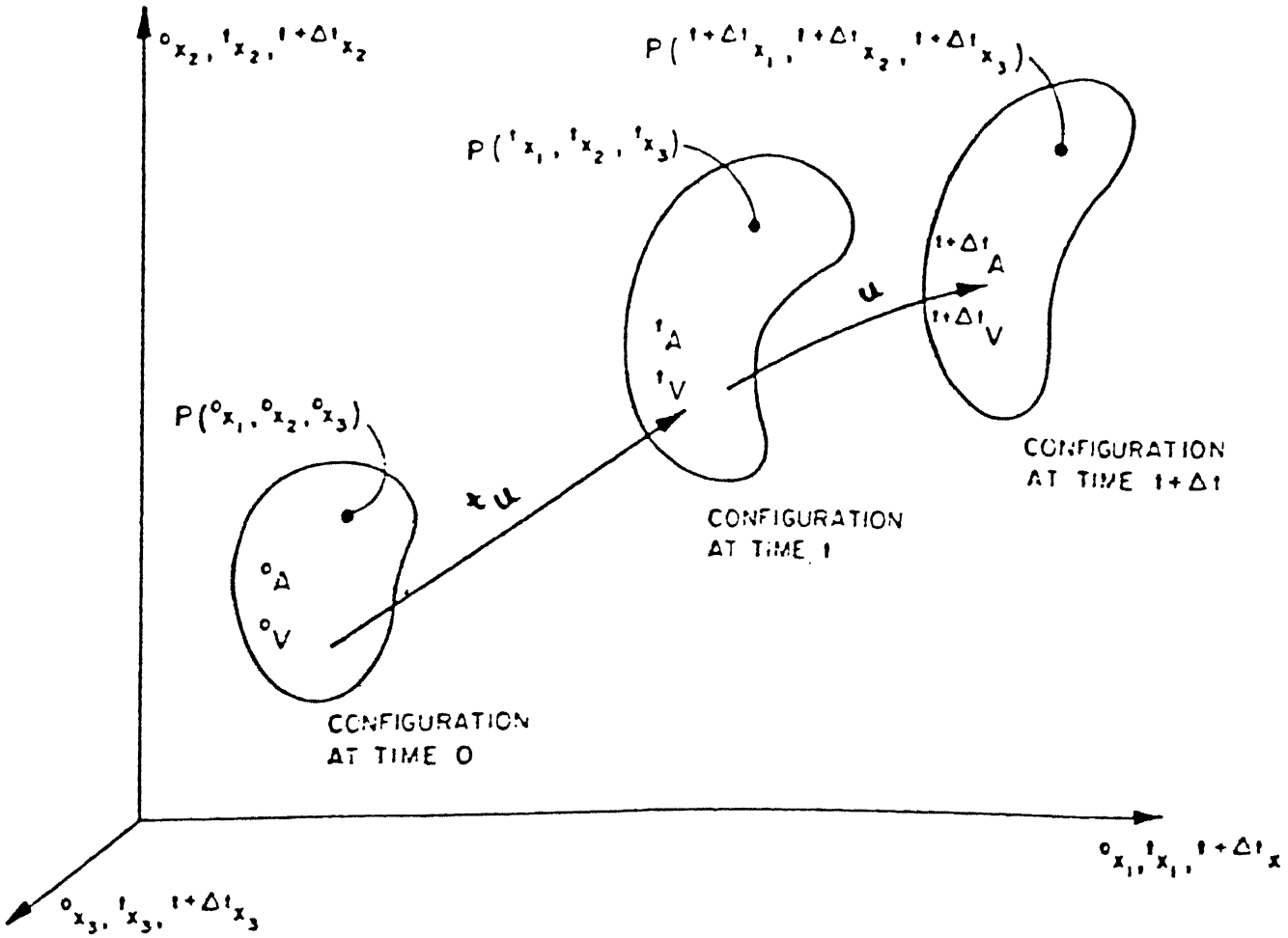

Figure 2.1: Motion of body in cartesian coordinate system

it is assumed that the displacements are so small that the configuration change is negligible.

The continuous change in the configuration of the body with loading in a large deformation analysis is dealt with in an elegant manner by using appropriate stress and strain measures, as discussed in the sections to follow.

2.1.2 Stress and Strain Tensors

As was pointed earlier, in the nonlinear analysis, special attention must be given to the fact that the configuration of the body changes continuously. This is taken care by choosing proper stress and strain measures. The stress and strain measures chosen should express the internal virtual work in equation (2.1) in terms of an integral over a volume that is known and it should be easy to incrementally decompose the stresses and strains in an effective manner. Though there are various stress and strain measures available, in principle, the stress and strain tensors that will be most suited for incremental formulation of virtual work principle are Second Piola-Kirchhoff stress tensor and Green-Lagrange strain tensor [15].

The Second Piola-Kirchhoff stress at time t referred to the configuration at time 0 is given by

$$ {}^{t}_{0}S_{ij} = \frac{{}^{0}\rho}{{}^{t}\rho} \; {}^{0}_{t}x_{i,m} \; {}^{t}\tau_{mn} \; {}^{0}_{t}x_{j,n} \tag{2.3} $$

where ${}^{0}_{t}x_{i,m} = \frac{\partial {}^{0}x_i}{\partial {}^{t}x_m}$ is the derivative of the coordinate in configuration at time 0 with respect to coordinate ${}^{t}x_m$ and $\frac{{}^{0}\rho}{{}^{t}\rho}$ represents the ratio of mass densities at time 0 and at time t. The determination of the ratio of mass densities is explained in the appendix. From equation (2.3) it can be seen that, by a purely kinematic transformation, the second Piola-Kirchhoff stress tensor at any configuration can be calculated from the corresponding cauchy stress tensor and vice versa.

The strain tensor used with the second Piola-Kirchhoff stress tensor in the large deformation analysis is the Green-Lagrange strain tensor and it is defined at any time t as

$$ {}^{t}_{0}\epsilon_{ij} = \frac{1}{2}({}^{t}_{0}u_{i,j} + {}^{t}_{0}u_{j,i} + {}^{t}_{0}u_{k,i} \; {}^{t}_{0}u_{k,j}) \tag{2.4} $$

in which ${}^{t}_{0}u_{i,j} = \frac{\partial {}^{t}u_i}{\partial {}^{0}x_j}$ is the derivative of the displacement component in configuration at time t with respect to coordinate ${}^{0}x_j$.

The stress and strain measures described are symmetric and their components are unaffected by rigid body rotations of the material [27]. A most important aspect is that the stress and strain tensors described above are energetically conjugate to each other [27], which is a necessary condition for using them in incremental formulations.

2.1.3 Total Lagrangian Formulation

Consider the deformation of the body starting from the configuration at time 0 to the configuration at time $t + \Delta t$ passing through discrete time steps Δt, $2\Delta t, \ldots$ as shown in the Fig.(2.1). In developing the solution for the virtual work expression (2.1) established in the configuration at time $t + \Delta t$, it is assumed that the solutions for the static and kinematic variables for all time steps starting from time 0 to time t, inclusive, have been obtained. The aim is to evaluate the solution variables at time $t + \Delta t$. After achieving this, the same strategy can then be applied repetetively till the complete solution path is solved. Hence, in the analysis the path of the body is followed from the original configuration (i.e. at $t = 0$) to the final configuration of the body. This method of approach is referred to as the lagrangian formulation [15] and widely used in the nonlinear analysis.

It was discussed in section 2.1.1 that the solution to virtual work expression (2.1) can be obtained if all the variables in the expression can be referred to some known configuration. For this purpose, in principle, any one of the already calculated equilibrium configurations could be used. However, the choice lies between two different formulations, namely, the total lagrangian formulation (T.L) and the updated Lagrangian formulation (U.L). In the total lagrangian formulation the solution variables in the configuration configuration $t+\Delta t$ can be obtained by referring all the variables to the undeformed equilibrium configuration at time 0. In the updated lagrangian formulation, the solution at time $t + \Delta t$ can be obtained from the configuration at time t i.e., the variables are all referred to the configuration at the end of the previous time step, which represents the load step in the case of static analysis.

The virtual work expression (2.1) can be transformed in terms of second Piola-Kirchhoff stress and Green-Lagrange strain as

$$\int_{{}^0V} {}_0^{t+\Delta t}S_{ij} \;\; \delta {}_0^{t+\Delta t}\epsilon_{ij} \;\; {}^0dV = {}^{t+\Delta t}R \tag{2.5}$$

where ${}_0^{t+\Delta t}S_{ij}$ are the cartesian components of the second Piola-Kirchhoff stress tensor and ${}_0^{t+\Delta t}\epsilon_{ij}$ are the cartesian components of the Green-Lagrange strain tensor at time $t + \Delta t$ referred to the configuration at time 0. In the analysis the load is

assumed to be deformation independent and hence ${}^{t+\Delta t}R$ is calculated using

$$ {}^{t+\Delta t}R = \int_{{}^{t+\Delta t}A} {}^{t+\Delta t}f_i \ \delta u_i \ {}^{t+\Delta t}dA \ + \ \int_{{}^{t+\Delta t}V} {}^{t+\Delta t}t_i \ \delta u_i \ {}^{t+\Delta t}dV \tag{2.6} $$

Approximate solutions to equations (2.5) and (2.6) can be obtained by linearizing the relations which is explained below.

1. Equation of Motion

$$ \int_{{}_0V} {}^{t+\Delta t}_{0}S_{ij} \ \delta {}^{t+\Delta t}_{0}\epsilon_{ij} \ {}^{0}dV = {}^{t+\Delta t}R \tag{2.7} $$

where

$$ {}^{t+\Delta t}_{0}S_{ij} = \frac{{}^{0}\rho}{{}^{t+\Delta t}\rho} \ {}^{0}_{t+\Delta t}x_{i,m} \ {}^{t+\Delta t}\tau_{mn} \ {}^{0}_{t+\Delta t}x_{j,n} \tag{2.8} $$

$$ \delta \ {}^{t+\Delta t}_{0}\epsilon_{ij} = \delta\frac{1}{2}({}^{t+\Delta t}_{0}u_{i,j} + {}^{t+\Delta t}_{0}u_{j,i} + {}^{t+\Delta t}_{0}u_{k,i} \ {}^{t+\Delta t}_{0}u_{k,j}) \tag{2.9} $$

2. Incremental Decompositions

   a) Stresses

$$ {}^{t+\Delta t}_{0}S_{ij} = {}^{t}_{0}S_{ij} + {}_0S_{ij} \tag{2.10} $$

   b) Strains

$$ \left.\begin{array}{l} {}^{t+\Delta t}_{0}\epsilon_{ij} = {}^{t}_{0}\epsilon_{ij} + {}_0\epsilon_{ij} \\ {}_0\epsilon_{ij} = {}_0e_{ij} + {}_0\eta_{ij} \end{array}\right\} \tag{2.11} $$

$$ \left.\begin{array}{l} {}_0e_{ij} = \frac{1}{2}({}_0u_{i,j} + {}_0u_{j,i} + {}^{t}_{0}u_{k,i} \ {}_0u_{k,j} + {}_0u_{k,i} \ {}^{t}_{0}u_{k,j}); \\ {}_0\eta_{ij} = \frac{1}{2}{}_0u_{k,i} \ {}_0u_{k,j}; \end{array}\right\} \tag{2.12} $$

   This can be derived using taylor's series

3. Equation of motion with Incremental decompositions

$$ \delta {}^{t+\Delta t}_{0}\epsilon_{ij} = \delta {}_0\epsilon_{ij} $$

$$ \int_{{}_0V} {}_0S_{ij} \ \delta {}_0\epsilon_{ij} \ {}^{0}dV + \int_{{}_0V} {}^{t}_{0}S_{ij} \ \delta {}_0\eta_{ij} \ {}^{0}dV = {}^{t+\Delta t}R - \int_{{}_0V} {}^{t}_{0}S_{ij} \ \delta {}_0e_{ij} \ {}^{0}dV \tag{2.13} $$

4. Linearisation of Equations of Motion

using the approximations

$$ {}_0S_{ij} = {}_0C_{ijrs}\ {}_0e_{rs}, \quad \delta_0\epsilon_{ij} = \delta_0 e_{ij}; $$

we obtain the approximate equation of motion:

$$ \int_{{}_0V} {}_0C_{ijrs}\ {}_0e_{rs}\ \delta_0 e_{ij}\ {}^0dV + \int_{{}_0V} {}^t_0S_{ij}\ \delta_0\eta_{ij}\ {}^0dV = {}^{t+\Delta t}R - \int_{{}_0V} {}^t_0S_{ij}\ \delta_0 e_{ij}\ {}^0dV \tag{2.14} $$

where

$$ {}_0C_{ijrs} = \lambda\ \delta_{ij}\ \delta_{rs} + \mu(\delta_{ir}\ \delta_{js} + \delta_{is}\ \delta_{jr}) $$

where λ and μ are Lame's constants and δ_{ij} is the kronecker delta.

$$ \lambda = \frac{E\ \nu}{(1+\nu)\ (1-2\nu)}; \quad \mu = \frac{E}{2(1+\nu)} $$

The relation (2.14) can be employed to calculate an increment in the dispacements, which then is used to evaluate approximations to the displacements, strains and stresses corresponding to $t + \Delta t$. The displacement approximations corresponding to $t + \Delta t$ are simply obtained by adding the calculated increments to the displacements of time t, and the strain approximations are evaluated from the displacements using the available kinematic relations i.e

$$ {}^t_0\epsilon_{ij} = \frac{1}{2}({}^t_0u_{i,j} + {}^t_0u_{j,i} + {}^t_0u_{k,i}\ {}^t_0u_{k,j}) $$

The stress can then be calculated using the constitutive relations for small strain

$$ {}^t_0S_{ij} = {}^t_0C_{ijrs}\ \ {}^t_0\epsilon_{rs} $$

Assuming that the approximate displacements, strains and thus stresses have been obtained we can now check into how much difference there is between the internal virtual work when evaluated with the calculated static and kinematic variables for time $t+\Delta t$ and the external work. Denoting the approximate values with a superscript

(1) in anticipation that an iteration will in general be necessary, the error due to linearisation is

$$Error = {}^{t+\Delta t}R - \int_{{}_0V} {}_0^{t+\Delta t}S_{ij}^{(1)} \ \delta_0^{t+\delta t}\epsilon_{ij}^{(1)} \ {}^0dV \tag{2.15}$$

The above considerations show that the R.H.S. in (2.14) represent an " out-of-balance virtual work " prior to the calculation of the increments in the displacements, where as the R.H.S. of (2.15) represent the " out-of-balance virtual work " after the solution, as the result of the linearisations performed. In order to further reduce the " out-of-balance virtual work " we need to perform an iteration in which the above solution step is repeated until the difference between the external virtual work and the internal virtual work is negligible within a certain convergence measure. Using the T.L. formulation the equation solved repetitively, for $k = 1, 2, 3, \ldots$ is

$$\int_{{}_0V} {}_0C_{ijrs} \ \Delta_0 e_{rs}^{(k)} \ \delta_0 e_{ij} \ {}^0dV + \int_{{}_0V} {}_0^tS_{ij} \ \delta\Delta_0\eta_{ij}^{(k)} \ {}^0dV =$$

$${}^{t+\Delta t}R - \int_{{}_0V} {}_0^{t+\Delta t}S_{ij}^{(k-1)} \ \delta_0^{t+\Delta t}\epsilon_{ij}^{(k-1)} \ {}^0dV \tag{2.16}$$

where the case $k = 1$ corresponds to the relation (2.14) and the displacements are updated as follows

$$\left.\begin{array}{l} {}^{t+\Delta t}u_i^{(k)} = {}^{t+\Delta t}u_i^{k-1} + \Delta u_i^{(k)} \\ {}^{t+\Delta t}u^{(0)} = {}^tu \end{array}\right\} \tag{2.17}$$

Equations above correspond to modified newton-iteration scheme.

2.1.4 Methodology for Elasto-Plastic Analysis

Before the onset of plastic yielding the relationship between the stress and strain is given by the standard linear elastic expression

$$\sigma_{ij} = C_{ijkl} \ \epsilon_{kl} \tag{2.18}$$

where σ_{ij} and ϵ_{kl} are the Second Piola-Kirchhoff stress and Green Lagrange strain components respectively and C_{ijkl} is the tensor of elastic constants which for an isotropic material has the form

$$C_{ijkl} = \lambda\ \delta_{ij}\ \delta_{kl} + \mu\ \delta_{ik}\ \delta_{jl} + \mu\ \delta_{il}\ \delta_{jk},$$

where λ and μ are the lame constants and δ_{ij} is the kronecker delta.

Plastic behavior is characterised by an irreversible straining which is not time dependent and which can only be sustained once a certain level of stress has been reached.

To model elasto-plastic material deformation three requirements have to be met:

- An explicit relationship between stress and strain under elastic conditions must be formulated.
- A yield criterion indicating the stress and strain level at which plastic flow commenses must be presented.
- A relationship between stress and strain must be developed for post yield behavior i.e when the deformation is made up of both elastic and plastic components.

The relationship between stress and strain under elastic conditions is given by (2.18).

Yield Criterion

The yield criterion determines the stress level at which plastic deformation begins and can be written in the general form

$$f(\sigma_{ij}) = K(k) \tag{2.19}$$

where f is some function and K is a material parameter (which may be a function of the hardening parameter k) to be determined experimentally. On physical grounds, any yield criterion should be independent of the orientation of the coordinate system employed and therefore it should be a function of the three stress invariants only.

$$\left.\begin{aligned} J_1 &= \sigma_{ii} \\ J_2 &= \tfrac{1}{2}\sigma_{ij}\sigma_{ij} \\ J_3 &= \tfrac{1}{3}\sigma_{ij}\sigma_{jk}\sigma_{ki} \end{aligned}\right\} \tag{2.20}$$

Experimental observations, notably by [28], indicate that plastic deformation of metals is essentially independent of hydrostatic pressure. Consequently the yield function can only be of the form

$$f(J_2', J_3') = K(k)$$

where J_2' and J_3' are the second and third invariants of the deviatoric stresses.

There are many yield criteria mentioned in the literature, but Tresca and Von Mises criteria are very popular.

Tresca Criteria

According to this criteria yielding begins when the maximum shear stress reaches a certain value. If the principal stresses are $\sigma_1, \sigma_2, \sigma_3$ where $\sigma_1 \geq \sigma 2 \geq \sigma 3$ then yielding begins when

$$\sigma_1 - \sigma_3 = Y(k) \tag{2.21}$$

where Y is a material parameter to be experimentally determined and which may be a function of the hardening parameter k.

Von Mises Criteria

Von Mises suggested that yielding occurs when J_2' reaches a critical value,

$$(J_2')^{1/2} = K(k) \tag{2.22}$$

in which K is a material parameter to be determined. J_2' can be explicitly written as

$$J_2' = \frac{1}{2}\ \sigma_{ij}'\ \sigma_{ij}' = \frac{1}{6}[(\sigma_1 - \sigma_2)^2 + (\sigma_2 - \sigma_3)^2 + (\sigma_3 - \sigma_1)^2] \tag{2.23}$$

Yield criterion may be further written as

$$\overline{\sigma} = \sqrt{3}\ (J_2')^{1/2} = \sqrt{3}\ K \tag{2.24}$$

where $\overline{\sigma} = \frac{\sqrt{3}}{2}\ \{\sigma_{ij}'\ \sigma_{ij}'\}^{1/2}$ is termed the effective stress.

Elasto-Plastic stress strain relation

After initial yielding the material behavior will be partly elastic and partly plastic. During any increment of stress, the changes of strain are assumed to be divisible into elastic and plastic components, so that

$$d\epsilon_{ij} = (d\epsilon_{ij})_e + (d\epsilon_{ij})_p \tag{2.25}$$

where

$$(d\epsilon_{ij})_e = \frac{\partial \sigma'_{ij}}{2\mu} + \frac{(1-2\nu)}{E}\,\delta_{ij}\,d\sigma_{kk} \tag{2.26}$$

In order to derive the relationship between the plastic strain component and the stress increment a further assumption on the material behavior must be made. It will be assumed that the plastic strain increment is proportional to the stress gradient of a quantity termed the plastic potential Q, so that

$$(d\epsilon_{ij})_p = d\lambda\,\frac{\partial Q}{\partial \sigma_{ij}} \tag{2.27}$$

where $d\lambda$ is a proportionality constant termed the plastic multiplier [29]. The above equation is termed the flow rule since it governs the plastic flow after yielding.

The identity $f \equiv Q$ gives us the normality condition[30]

$$(d\epsilon_{ij})_p = d\lambda\,\frac{\partial f}{\partial \sigma_{ij}} \tag{2.28}$$

and is termed the normality condition since $\frac{\partial f}{\partial \sigma_{ij}}$ is a vector directed normal to the yield surface at the stress point under consideration. Experimental observations indicate that the normality condition is an acceptable assumption for metals.

Substituting $(d\epsilon_{ij})_e$ and $(d\epsilon_{ij})_p$ in (2.25) gives

$$(d\epsilon_{ij}) = \frac{\partial \sigma'_{ij}}{2\mu} + \frac{(1-2\nu)}{E}\,\delta_{ij}\,d\sigma_{kk} + d\lambda\,\frac{\partial f}{\partial \sigma_{ij}} \tag{2.29}$$

For matrix formulation the yield function $f(\sigma) = K(k)$ can be rewritten as

$$f(\sigma) - K(k) = 0$$

or

$$F(\sigma,\ k) = f(\sigma) - K(k) \tag{2.30}$$

By differentiating we have

$$dF = \frac{\partial F}{\partial \sigma}\,d\sigma + \frac{\partial F}{\partial k}\,dk = 0, \tag{2.31}$$

or

$$a^T \; d\sigma - A \; d\lambda = 0 \tag{2.32}$$

where

$$a^T = \frac{\partial F}{\partial \sigma} = [\frac{\partial F}{\partial \sigma_x}, \quad \frac{\partial F}{\partial \sigma_y}, \quad \frac{\partial F}{\partial \tau_{xy}}] \tag{2.33}$$

and

$$A = -\frac{1}{d\lambda} \frac{\partial F}{\partial k} \, dk \tag{2.34}$$

Therefore, equation (2.29) reduces to

$$d\epsilon = [D]^{-1} d\sigma + d\lambda \frac{\partial F}{\partial \sigma} \tag{2.35}$$

where $[D]$ is the matrix of elastic constants. Premultiplying both sides of (2.35) by $d_D = a^T \; D$ and eliminating $a^T \; d\sigma$ by use of (2.32) we obtain the plastic multiplier

$$d\lambda = \frac{1}{[A + a^T \; D \; a]} \; a^T \; d_D \; d\epsilon$$

Substituting this in (2.35) we get the complete elasto-plastic incremental stress strain relation to be

$$d\sigma = D_{ep} \; d\epsilon,$$

where

$$D_{ep} = D - \frac{D \;\; a \;\; a^T \;\; D}{A + a^T \;\; D \;\; a}$$

It can be shown that [30]

$$A = H' = \frac{\partial \sigma}{\partial \epsilon_p}$$

which is the local slope of uniaxial stress/plastic strain curve and can be determined experimentally from

$$H' = \frac{E_T}{1 - \frac{E_T}{E}}$$

where E_T is the elastic-plastic tangent modulus of uniaxial stress-strain curve.

Chapter 3

FINITE ELEMENT IMPLEMENTATION

In the previous chapter the incremental continuum mechanics equations that form the basis of general nonlinear displacement based finite element analysis were presented. In this chapter we use these equations to develop the governing finite element equations. The numerical evaluation of elasto-plastic material matrix will also be explained. At the end the numerical algorithms employed in solving resulting nonlinear finite element equations and the convergence criteria are dealt with.

3.1 Isoparametric finite element discretisation

By invoking the principle of virtual displacements for each of the nodal point displacements in turn, the governing finite element equations are obtained. The basic steps in the derivation of the governing finite element equations are the same as those used in linear analysis: the selection of the interpolation functions and the interpolation of the element coordinates and displacements with these functions in the governing continuum mechanics equations.

In the incremental nonlinear analysis, since the new element coordinates are obtained by adding the element displacements to the original coordinates, it follows that the use of the same interpolations for the displacements and coordinates represent a consistent solution approach.

Since the aim of the present work is to evaluate the effect of geometric nonlinearity on fracture parameters for two dimensional plane stress/plane strain conditions, attempt is made here to develop the finite element matrices for 8-noded isoparametric element with two degrees of freedom (u, v) at each node.

Consider an 8-noded element in the configuration at time 0 and at time t in the

global coordinate system as shown in Fig. 3.1. In the isoparametric element solution, the coordinates and displacements are interpolated using

$$\left.\begin{array}{l} {}^{0}x_i = \sum_{k=1}^{N} \; h_k \; {}^{0}x_i^k \\ {}^{t}x_i = \sum_{k=1}^{N} \; h_k \; {}^{t}x_i^k \\ {}^{t+\Delta t}x_i = \sum_{k=1}^{N} \; h_k \; {}^{t+\Delta t}x_i^k \\ i = 1,2 \end{array}\right\} \tag{3.1}$$

$$\begin{array}{l} {}^{t}u_i = \sum_{k=1}^{N} \; h_k \; {}^{t}u_i^k \\ i = 1,2 \end{array} \tag{3.2}$$

where ${}^{t}x_i^k$ is the coordinate of nodal point k corresponding to direction i at time t and ${}^{t}u_i^k$ is the displacement of nodal point k corresponding to direction i at time t. h_k is the interpolation function corresponding to nodal point k and N is the number of element nodal points.

Using equations (3.1) and (3.2) in equation (2.14) to evaluate the displacement derivatives required in the integrals, we get considering a single element

$$({}_{0}^{t}K_L \; + \; {}_{0}^{t}K_{NL}) \; (\Delta u^{(i)}) \; = \; {}^{t+\Delta t}R \; - \; {}_{0}^{t+\Delta t}F^{(i-1)} \tag{3.3}$$

where ${}_{0}^{t}K_L$ is linear strain incremental stiffness matrix,

${}_{0}^{t}K_{NL}$ is Nonlinear strain (geometric or initial stress or tangent) incremental stiffness matrix,

${}_{0}^{t+\Delta t}F^{(i-1)}$ is vector of nodal point forces equivalent to the element stresses at time t $+\Delta t$ and iteration $(i-1)$ and

${}^{t+\Delta t}R$ is vector of externally applied nodal point loads at time $t+\Delta t$.

and

$$\left.\begin{array}{l} {}_{0}^{t}K_L \; \tilde{u} = (\int_{{}^{0}V} \; {}_{0}^{t}B_L^T \; {}_{0}C \; {}_{0}^{t}B_L \; {}^{0}dV) \; \tilde{u} \\ {}_{0}^{t}K_{NL} \; \tilde{u} = (\int_{{}^{0}V} \; {}_{0}^{t}B_{NL}^T \; {}_{0}^{t}S \; {}_{0}^{t}B_{NL} \; {}^{0}dV) \; \tilde{u} \\ {}_{0}^{t}F = \int_{{}^{0}V} \; {}_{0}^{t}B_L^T \; {}_{0}^{t}\tilde{S} \; {}^{0}dV \end{array}\right\} \tag{3.4}$$

${}_{0}^{t}K_L$, ${}_{0}^{t}K_{NL}$ and ${}_{0}^{t}F$ are obtained from

$$\left.\begin{array}{l} \int_{{}^{0}V} \; {}_{0}C_{ijrs} \; {}_{0}e_{rs} \; \delta_{0}e_{ij} \; {}^{0}dV \\ \int_{{}^{0}V} \; {}_{0}^{t}S_{ij} \; \delta_{0}\eta_{ij} \; {}^{0}dV \\ \int_{{}^{0}V} \; {}_{0}^{t}S_{ij} \; \delta_{0}e_{ij} \; {}^{0}dV \end{array}\right\} \tag{3.5}$$

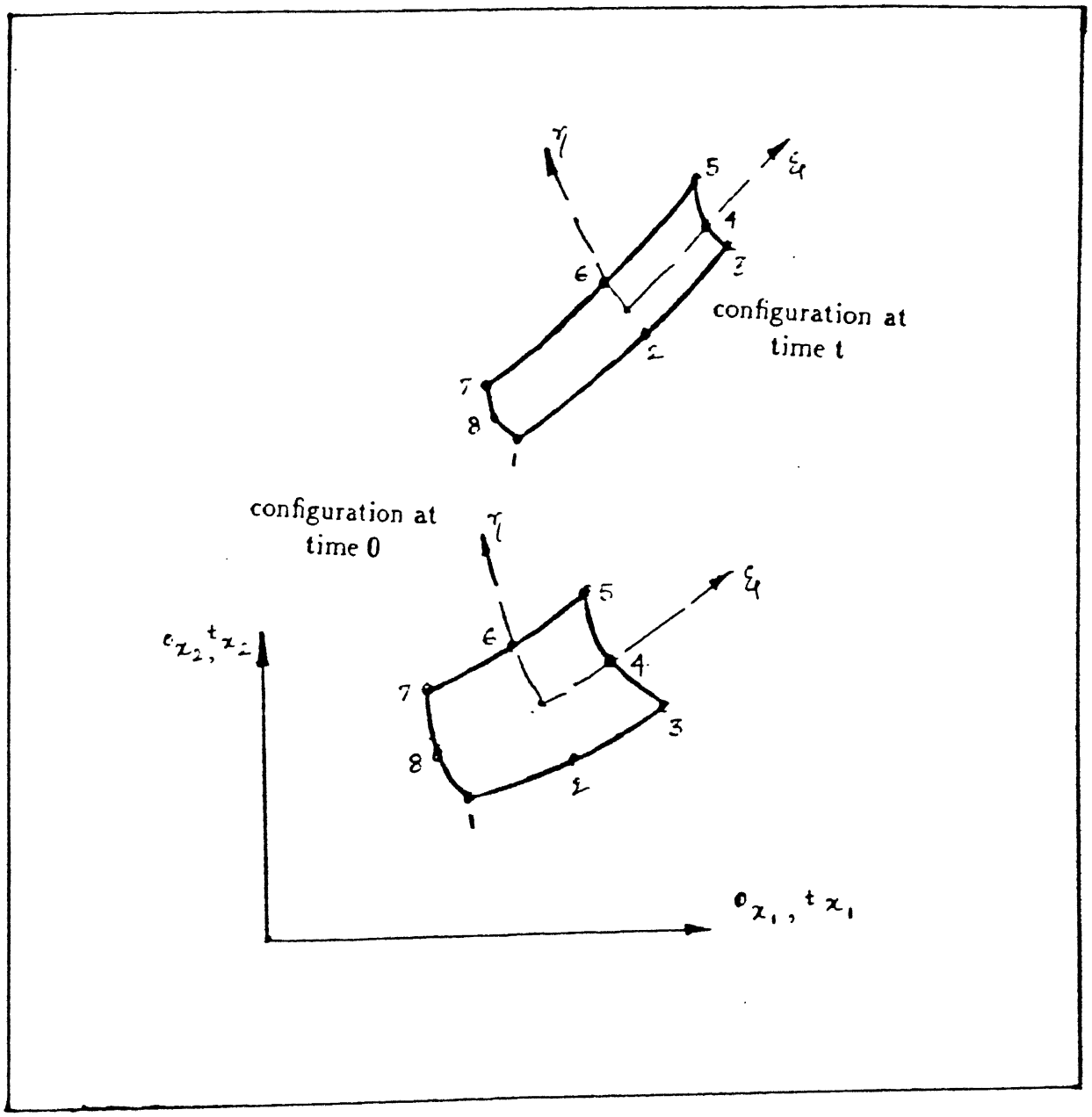

Figure 3.1: Two dimensional element in the global plane

respectively. 3 x 3 gaussian integration is used in the present analysis to evaluate the linear and nonlinear stiffness matrices.

The explicit form of the finite element matrices are given in the appendix.

3.2 Numerical Computation of Elasto-plastic material matrix

For numerical computations it is convinient to rewrite the yield criteria considered in chapter 2 in terms of alternative stress invariants. This formulation is due to [31] and its main advantage is that it permits the computer coding in a general form and necessiates only the specification of three constants for any individual criterion.

We define a parameter θ to be a convinient alternative to the third invariant J_3' . The physical interpretation of θ is evident from Fig. 3.2.

Based on these alternative stress invariants we can rewrite the Tresca and Von Mises yield criterion as

$$2\ (J_2')^{1/2}\ \ cos\theta = \sigma_Y(k) \tag{3.6}$$

and

$$\sqrt{3}\ (J_2')^{1/2} = \sigma_Y(k) \tag{3.7}$$

respectively.

In order to calculate the elasto-plastic material matrix we require to express the flow vector 'a' in a form suitable for numerical computation. It can be shown that the flow vector

$$a^T = \frac{\partial F}{\partial \sigma} =$$

$$\frac{\partial F}{\partial J_1}\ \frac{\partial J_1}{\partial \sigma} + \frac{\partial F}{\partial (J_2')^{1/2}}\ \frac{\partial (J_2')^{1/2}}{\partial \sigma} + \frac{\partial F}{\partial \theta}\ \frac{\partial \theta}{\partial \sigma}\ ,$$

can be written as [30]

$$a = c_1\ \ a_1 + c_2\ \ a_2 + c_3\ \ a_3 \tag{3.8}$$

where

$$a_1{}^T = \{1,\ \ 1,\ \ 0\}$$

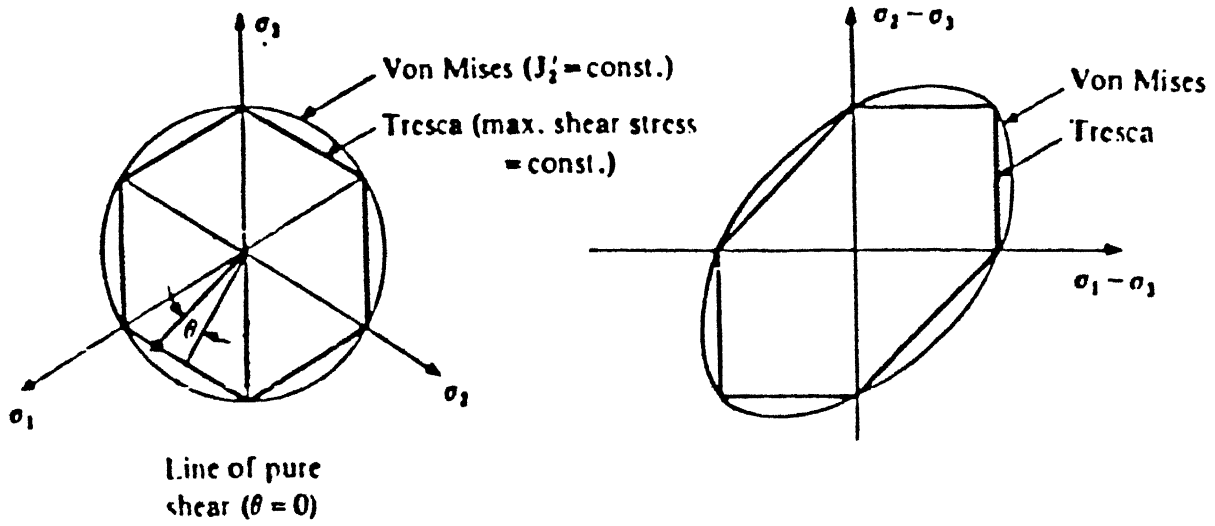

Figure 3.2: Two dimensional representations of the Tresca and Von Mises yield criteria

$$a_2{}^T = \frac{1}{2J_2'^{1/2}} \{\sigma_x, \ \sigma_y, \ 2\tau_{xy}\}$$

$$a_3{}^T = \{(\frac{J_2'}{3}), (\frac{J_2'}{3}), (\sigma_x \ \ \sigma_y - \tau_{xy}{}^2 + \frac{J_2'}{3})\},$$

and

$C_1 = 0 \ \ C_2 = 2 \ cos\theta(1 + tan\theta \ \ tan3\theta) \ \ C_3 = \frac{\sqrt{3}}{J_2'} \ (\frac{sin\theta}{cos3\theta})$ for tresca criterion.

$C_1 = 0 \ \ C_2 = \sqrt{3} \ \ C_3 = 0$ for Von Mises criterion.

Thus the elasto-plastic material matrix can be determined from

$$D_{ep} = D - \frac{D \ \ a \ \ a^T \ \ D}{A + a^T \ \ D \ \ a}$$

where $A = H'$ the strain hardening parameter.

Once the large deformation analysis is implemented and the elasto-plastic material matrix is calculated, assuming small strains large elastic plastic deformations can be modeled by simply substituting the Second Piola Kirchhoff stress tensor and Green-Lagrange strains in the material characterisation for the small displacement engineering stress and strain measures.

3.3 Numerical Procedures for the solution of Non-linear finite element equations

Having carried out the selection of appropriate finite element model, for the nonlinear analysis, a reliable and accurate response prediction of the model is essential to make use of the results with confidence. In the incremental solution procedure, it is of utmost importance to satisfy the governing finite element equations in each load increment to sufficient accuracy. Otherwise, the solution errors may accumulate and lead to solution instabilities.

The basic equations to be solved in the nonlinear analysis corresponding to time $t + \Delta t$ are

$$^{t+\Delta t}R(u^*) - {}^{t+\Delta t}F(u^*) = 0 \tag{3.9}$$

where ${}^{t+\Delta t}R$ is the vector of externally applied nodal point loads corresponding to time $t + \Delta t$ and ${}^{t+\Delta t}F$ is the internal force vector in the same configuration. If the load increments are small the approximate equation to be solved reduces to

$$ {}^{t+\Delta t}R - {}^{t}F = 0 $$

But if a large increment is used the solution of equation (3.9) involves iteration.

Two methods are widely used in solving nonlinear finite element analysis equations: Newton-Raphson and the Modified Newton-Raphson method. The only difference between these two methods is that in Newton-Raphson method the stiffness matrix is updated in every iteration, whereas Modified Newton-Raphson method employs lesser number of stiffness updations and hence may need more number of iterations than the full Newton-Raphson method. The details about these two methods are explained in [27].

3.4 Convergence criteria

In an incremental solution procedure, a realistic criteria to terminate the iteration process is important. After the solution variables are obtained after each iteration, a check has to be made to see whether the solution has converged within the specified tolerance.

The tolerance can be specified on displacements, forces or stresses: at the end of each iteration a check is made to see whether the increment in displacement, or norm of out of balance load vector or increment in stresses is within specified tolerance respectively.

In the present work the criterion for convergence is based on out of balance forces at the end of each iteration. This can be explained as

$$ \frac{\sqrt{\sum_{i=1}^{N} (\psi_i^r)^2}}{\sqrt{\sum_{i=1}^{N} (f_i)^2}} \; X \; 100 \; \leq TOLER $$

where N is the total number of nodal points in the problem and r denotes the iteration number.

$f_i's$ are the applied forces and $\psi_i's$ are the residual forces.

This criterion states that convergence occurs if the norm of the residual forces becomes less than $TOLER$ times the norm of the total applied force. The multiplication factor of 100 on the left hand side allows the specified tolerance factor to be considered as a percentage term.

The tolerance should be specified in such a way that the results should be obtained with sufficient accuracy but at the same time the process should not become computationally expensive.

3.5 Program Implementation

This section deals with the computational steps involved in developing the software for modelling large elastic plastic deformations of two dimensional plane stress/plane strain problems. The algorithm is presented with reference to the Newton-Raphson and Modified Newton-Raphson technique.

Computational Steps: Iteration number is represented by i and load increment by m. At start, $m = 1$ and $i = 1$.

1. Reading the applied incremental force vector so that the total external force is given by ${}^{m}R = {}^{m-1}R + {}^{m}\{\Delta R\}$.

2. Checking if the iterative technique is Modified Newton-Raphson method and $m \neq 1$. If Yes, go to step 4, else the full Newton-Raphson method is employed by going to step 3.

3. Calculating the overall stiffness matrix ${}^{m}[K] = {}^{m}[K]_L + {}^{m}[K]_{NL}$ for the structure using the equations developed in this chapter. The elements of linear and nonlinear strain displacement transformation matrices used in the determination of the linear and nonlinear stiffness matrices are given in the appendix. The elastic or elasto-plastic material matrix has to be accordingly used depending on whether an individual element has yielded or not.

4. Solving for the incremental displacements u in equation (3.3) where ${}^{m}R$ is the force vector used in the R.H.S.

5. Calculating the incremental displacements, strains and stress components.

6. Calculating the total stresses at the end of iteration i of load increment m.

7. Finding the equilibrium force vector using stress vector calculated in step 6.

8. Using the force criterion to check for convergence.
9. If the solution has converged proceed with next load increment else find unbalanced force vector and go to step 2.

Stop when all load increments are finished.

Chapter 4

EVALUATION OF FRACTURE PARAMETERS

Cracks are present to some degree in all structures. They may exist as basic defects in the constituent materials or they may be induced in construction or during service life. Therefore, to prevent failure by crack propogation it is necessary to evaluate fracture parameters. The fracture parameters considered in the present study are Energy release rate and CTOD. Analytical solutions exist for selected, relatively simple, cases, and it is in the determination of the stress and displacement fields for complex practical situations that numerical techniques such as finite elements and boundary integral methods play an important role [32]. Crack tip singularity modeling is discussed in section 4.1. Estimation of fracture parameters is discussed in section 4.2.

4.1 Crack Tip Singularity Modeling

LEFM studies have shown that the stresses nearer to the cracktip vary inversely with the square root of the radial distance (r) from the crack tip. This implies that the stresses at the crack tip posses $1/\sqrt{r}$ singularity. For a elastic perfectly plastic material once we come to the plastic region stresses at the crack tip posses 1/r singularity. For a material with strain hardening the singularity is of the type $1/r^n$ where $.5 < n < 1$. So elements near the crack tip should be able to model $1/\sqrt{r}$ singularity while within the elastic limit and 1/r singularity after crossing the elastic limit.

This singularities can be modeled in a two dimensional 8-noded isoparametric element by

* shifting the mid side nodes near the crack tip to the quarter point as shown in Fig. 4.1.b [16-19].

* Collapsing an edge of the element to a single node at the crack tip [16-19] apart from shifting the mid side nodes to the quarter point to form triangular crack tip elements as shown in Fig. 4.1.c.

To model $1/\sqrt{r}$ singularity the collapsed nodes are constrained to move as a single point and no relative movement between the nodes is allowed. To model 1/r singularity three nodes which are constrained to move as a single point are released so that relative movement between them is possible.

Using the above procedure the singularity is modeled in the interior as well as on the boundary of the element.

4.2 Estimation of Fracture parameters

In the study of structural problems involving cracks, the aim is to find the load at which the crack growth starts initiation leading to the ultimate failure of the structure. In EPFM J-integral and CTOD are the two widely used fracture parameters.

The fracture parameter called the J-integral developed in [33] which is essentially the energy released per unit crack extension per unit thickness of the cracked body. This parameter is applicable to elastic or elasto-plastic behavior.

The two dimensional form of the J-integral, with reference to crack problems, is given by

$$J = \int_{\Gamma} \left[W \, dy - T \, \frac{\partial u}{\partial x} \, ds \right]$$

with $W(\epsilon) = \int_0^{\epsilon} \sigma_{ij} \; d\epsilon_{ij}$ where Γ is an arbitrary contour around the crack tip starting from one face and ending at the opposite face of the crack (fig. 4.2)

ds is an element of arc along the integration contour,

T is the traction vector.

u is the displacement vector.

The value of J is independent of the actual path chosen provided that the initial and end points of contour are on the opposite faces of the crack and that crack faces are stress free.

It has also been shown [33] that J-integral, when defined along a contour around

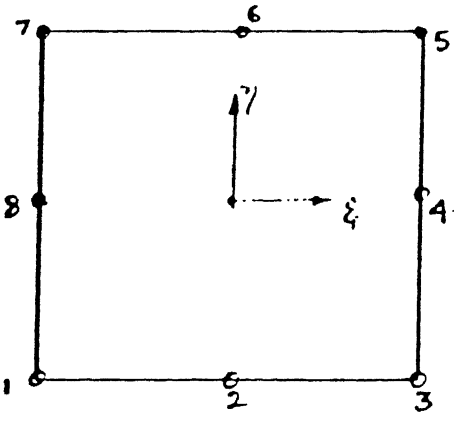

a.Parent element

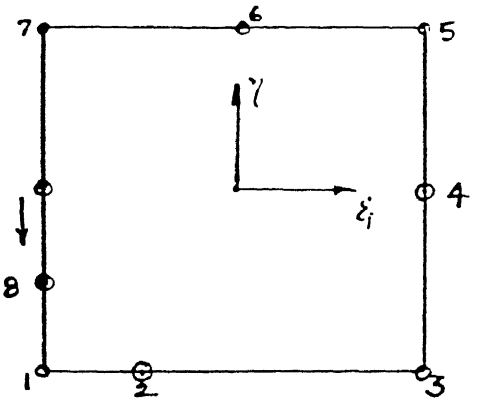

b.Quarter point element

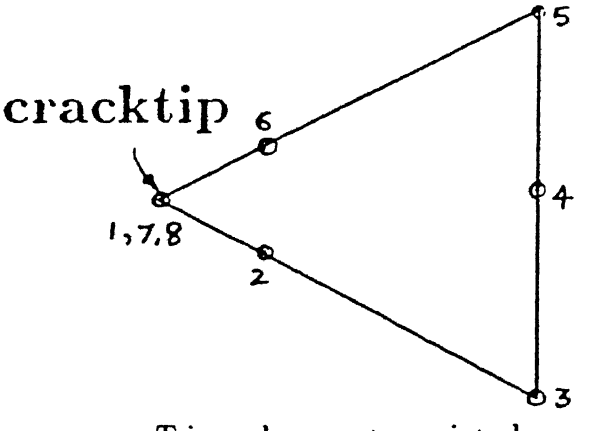

c.Triangular quarter point element

Figure 4.1: Cracktip singular elements

the crack tip represents the change in potential energy for unit crack area extension da.

i.e $J = -\frac{\partial V}{\partial a}$

where V is the potential energy. Crack growth or fracture is said to occur for a particular load when the J value for the given loading conditions exceeds a critical value J_{1C} which is a material constant.

The method used for evaluation of *EnergyReleaseRate* in the present study is given below.

Consider the load-displacement diagram for a crack of size 'a' represented by the curve OA in Fig. 4.3. For a crack of size 'a+da' the load displacement diagram is shown by the curve OE. Suppose the crack extension from a to $a + da$ takes place for a particular load P. Then, the Energy Release Rate for that particular load P by the crack extension da is given by the area between the two curves divided by $B\ da$ where B is the thickness of the body.

Once the displacement field near the crack tip is known the crack tip opening displacement can be found out.

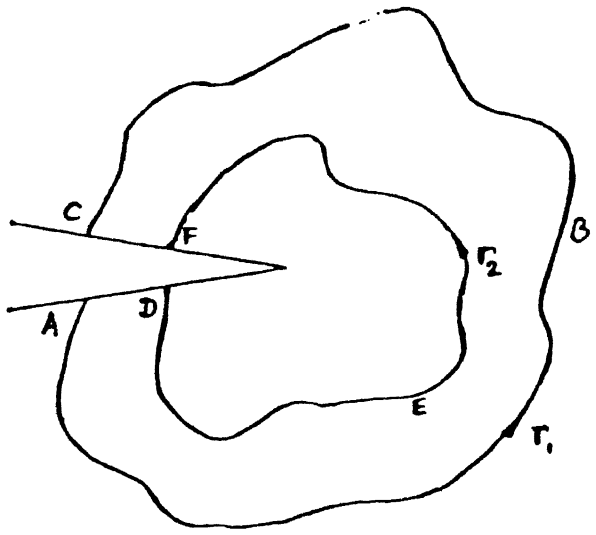

Fig. 4.2 Contour around cracktip

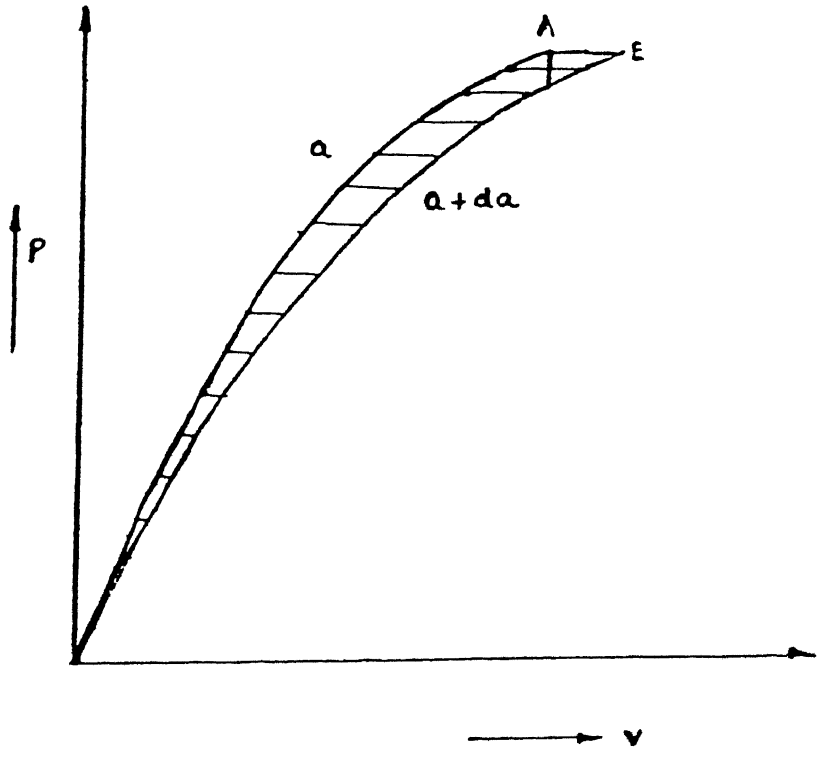

Fig. 4.3 Load-Displacement diagram for cracked body

Chapter 5

RESULTS AND DISCUSSION

Some sample problems are solved using the program developed. They are discussed in this chapter. Three problems are solved for bodies having cracks. In these problems the effect of geometric nonlinearity on fracture parameters is reported.

a) Cantilever Subjected to Moment at its Free End

A geometric nonlinear analysis is carried out for a cantilever subjected to a moment at its free end. Fig. 5.1 gives the details of the geometry and the material properties used in the analysis.

The moment is simulated using two equal and opposite forces at the free end of the cantilever as shown in Fig. 5.2. Since the loading is applied in steps the forces have to be follower forces. This is simulated in the program. The cantilever is modelled using 20 8-noded isoparametric plane stress elements. The mesh is shown in Fig. 5.3. The same problem is analytically solved in [34]. Results obtained using our program are compared with the analytical solution. Good agreement with the results is evident from Table 5.1 and Table 5.2. Displacement is in cm and Moment is in N cm.

Table 5.1: Comparision of Axial displacement

Moment	Analytical	Present Work
36.65	.6	.6003
73.30	1.187	1.187
109.95	2.06	2.06
146.60	3.17	3.175
183.25	4.8	4.45

Table 5.2: Comparision of Transverse displacement

Moment	Analytical	Present Work
36.65	5.14	5.14
73.30	10.15	10.15
109.95	14.93	14.93
146.60	20.00	19.375
183.25	25.0	23.45

a) Cantilever Subjected to End Moment

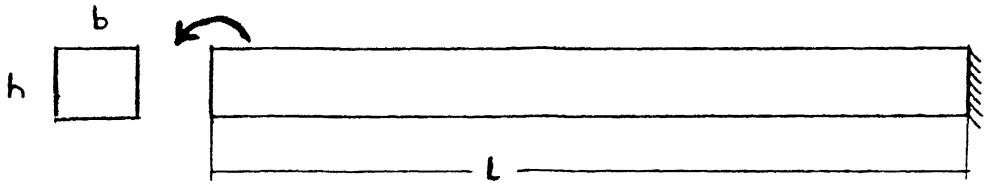

Dimensions l = 100 cm b = 20 cm h = 1 cm

Properties E = 2.1 x 10^4 N/cm^2 $\nu = 0.0$

Figure 5.1: Cantilever subjected to end moment

Fig. 5.4 shows the load deflection response and Fig. 5.5 shows the deformed shape of the cantilever.

b) Large deflection analysis of an Arch

A large deflection analysis of an arch fixed at both ends is carried out using the program developed. The arch is subjected to a point load at the middle as shown in Fig. 5.6. Considering the symmetry of the problem only one half (left half) of the arch is modelled. The finite element mesh is composed of 12 8-noded isoparametric plane stress elements as shown in Fig. 5.7. Fig. 5.8 shows the final deformed shape of the arch. Fig. 5.9 shows the load deflection response of the arch. It can be seen that the arch stiffens with increasing load.

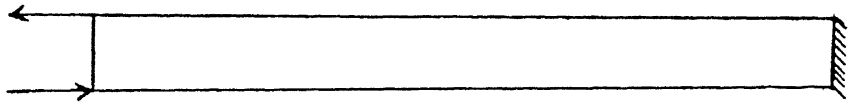

Figure 5.2: Moment on Cantilever

Problems involving Cracked Bodies

The Elastic Plastic material matrix whose formulation was explained in section 2.1.4 was validated with the help of results available in literature. After such validation the effect of geometric nonlinearity on fracture paramters was investigated.

c) Simply Supported Beam with a Central Crack under Point load

A simply supported beam with a central crack subjected to central point load is investigated to study the effect of geometric nonlinearity on fracture parameters. Fig. 5.10 gives the dimensions and material properties used in the analysis. P_o is the total applied load. It is assumed that the material is elastic and perfectly plastic.

Fig. 5.11 shows the mesh used for finite element analysis. Considering the symmetry of the problem only one half of the beam is modelled. The structure is decomposed into 96 8-noded plane stress elements for analysis. To model crack tip singularity the analysis uses triangular quarter point 8-noded isoparametric elements as explained in section 4.1. Before adopting this mesh to study the effect of geometric nonlinearity on fracture parameters, a convergence study was carried out using three meshes. The first mesh had 64 elements and 231 nodes, the second mesh consisted of 96 elements and 335 nodes and the third mesh had 144 elements and 491 nodes. We observed a

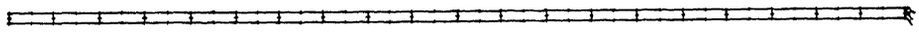

Figure 5.3: Finite element mesh of cantilever

—— Axial Displacement

- - - - - - Transverse Displacement

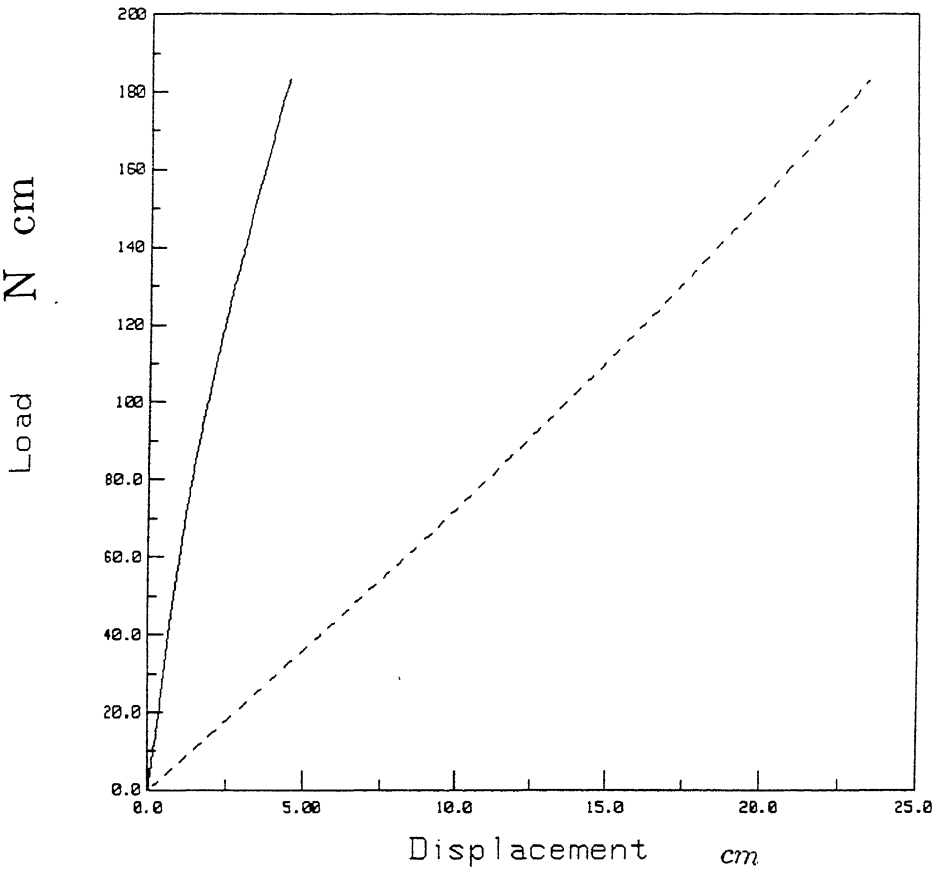

Figure 5.4: Load deflection response of cantilever

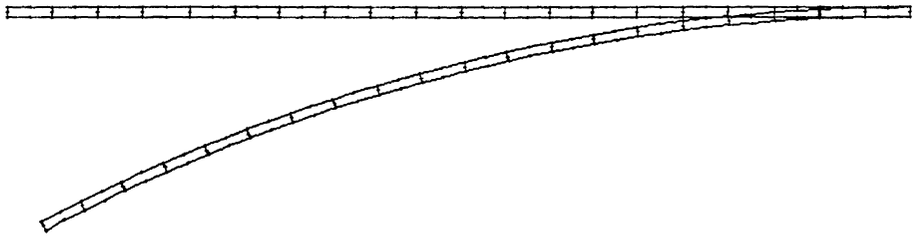

Figure 5.5: Deformed shape of cantilever

b) Large deflection analysis of an arch

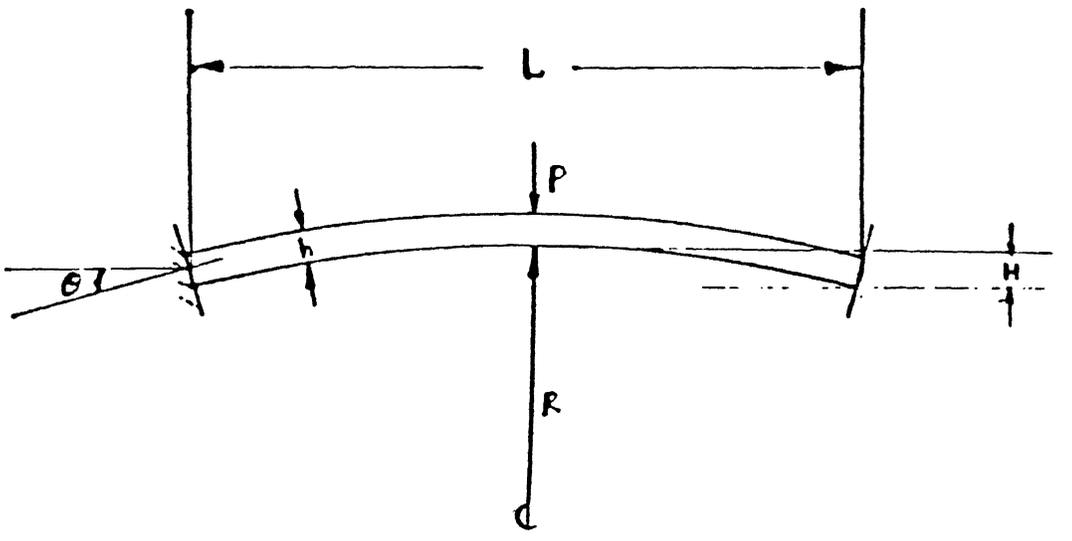

Dimensions:

L =	863 mm (34.0 in)	R =	3.380 m (133.1 in)
H =	27.9 mm (1.09 in)	b =	25.4 mm (1 in)
θ =	7.334°	h =	4.8 mm (.1875 in)

Properties:

E = 68.948E4 MPa (1.0E8 psi)

ν = 0.2

Figure 5.6: Arch under Point load

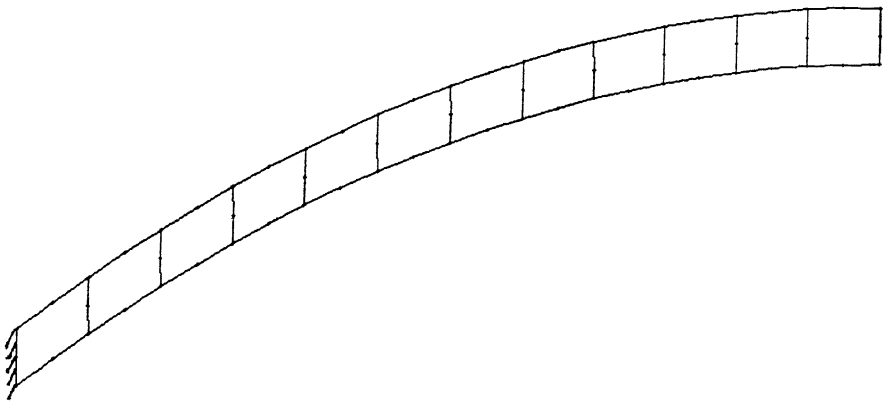

Figure 5.7: Finite element mesh of Arch

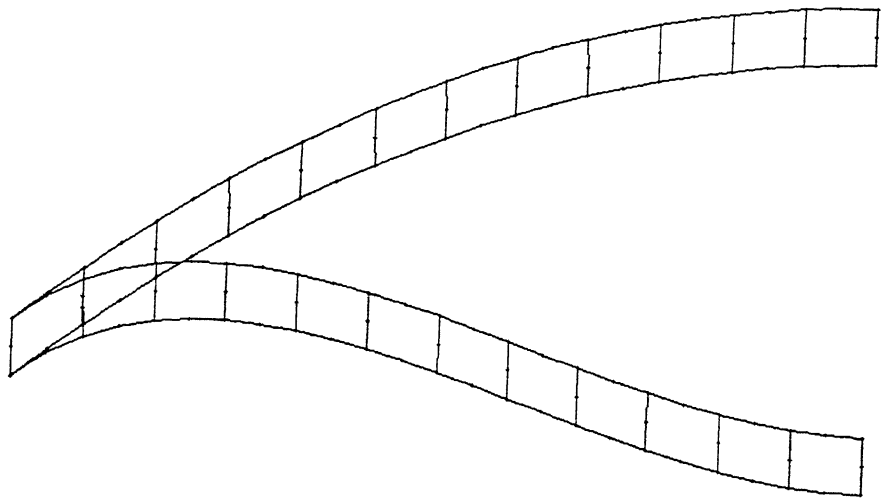

Figure 5.8: Deformed shape of Arch

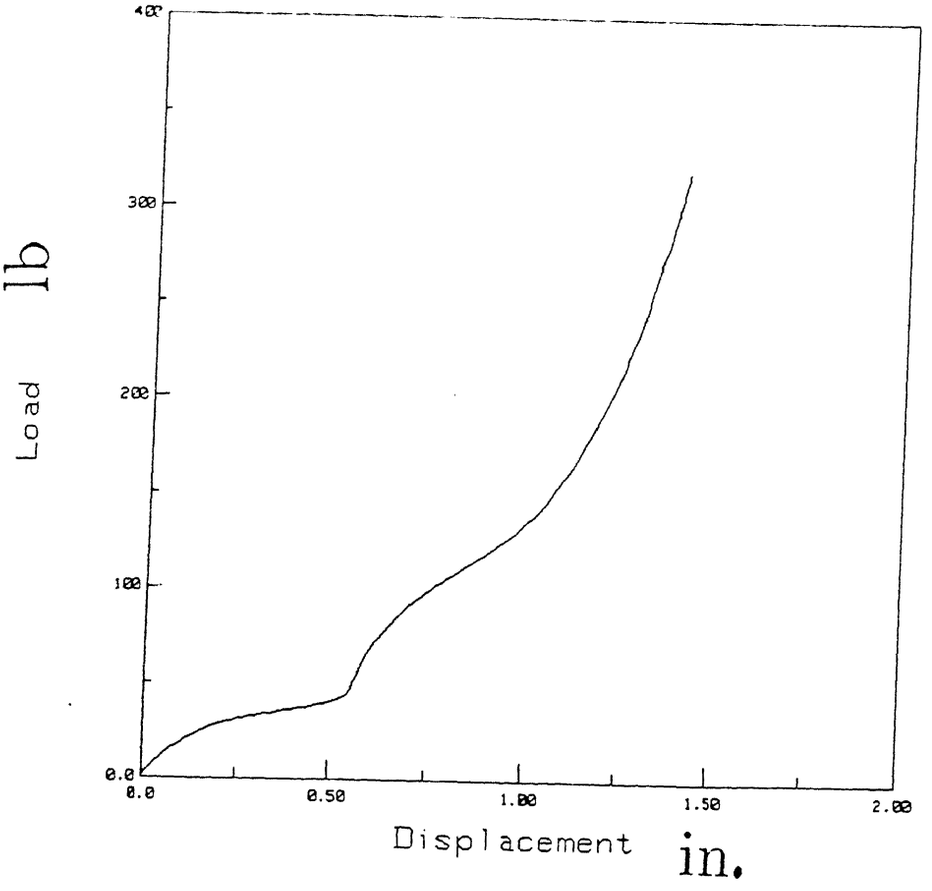

Figure 5.9: Load deflection response of Arch

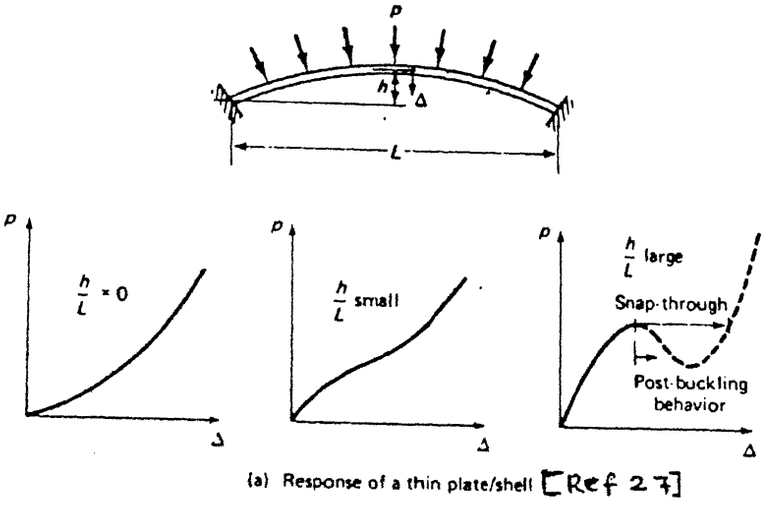

(a) Response of a thin plate/shell [Ref 27]

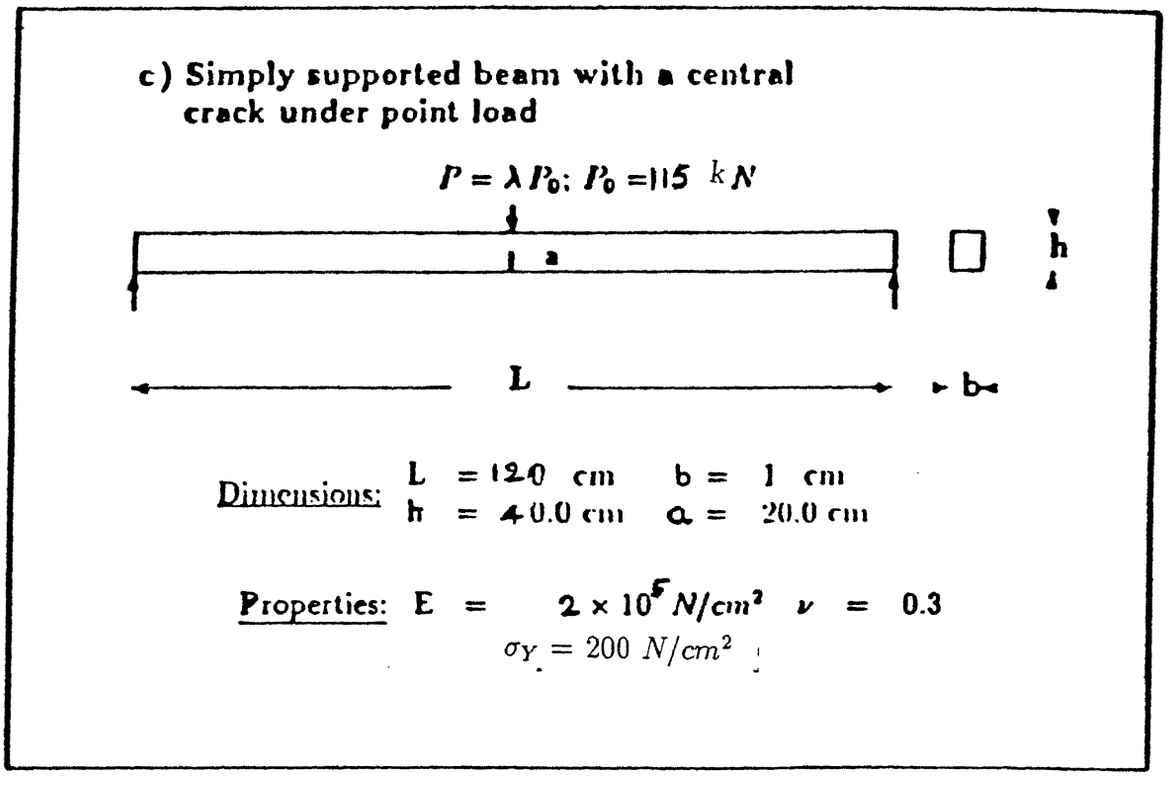

Figure 5.10: Simply supported beam under point load

monotonic convergence and there was no mesh dependence on the results. Considering computational efficiency and accuracy we adopted the second mesh i.e with 96 elements and 335 nodes for further analysis.

The effect of geometric nonlinearity on energy release rate is shown in Fig. 5.12 and the effect of geometric nonlinearity on CTOD is shown in Fig. 5.13. The plastic zone near the crack is shown in Figs. 5.14a, 5.14b and 5.14c. The plastic zone at limit load is shown in Fig. 5.15

d) Center cracked plate under uniaxial loading

A problem of center cracked plate of finite size subjected to uniaxial loading is considered here for analysis. The objective is to evaluate the effect of geometric nonlinearity on fracture parameters.

The geometry and material properties of the plate are shown in Fig. 5.16. P_o is the total applied load. Because of symmetry, a quarter of the plate shown in Fig. 5.16 is taken for analysis. The finite element mesh is shown in Fig 5.17. The singularity at the crack tip is modelled by the use of triangular crack tip elements. It is assumed that the material is elastic and perfectly plastic.

The effect of geometric nonlinearity on energy release rate and CTOD is shown in Figs. 5.18 and 5.19. The plastic zone near the crack is shown in Figs. 5.20a, 5.20b and 5.20c.

e) Edge cracked plate under uniaxial loading

A problem of edge cracked plate of finite size subjected to uniaxial loading considered here for analysis. The objective is to evaluate the effect of geometric nonlinearity on fracture parameters.

The geometry and material properties of the plate are shown in Fig. 5.21. P_o is the total applied load. Because of symmetry, half of the plate shown in Fig. 5.21 is taken for analysis. The finite element mesh is shown in Fig 5.22. The singularity at the crack tip is modelled by the use of triangular crack tip elements. It is assumed that the material is elastic and perfectly plastic.

The effect of geometric nonlinearity on energy release rate and CTOD is shown in Figs. 5.23 and 5.24. The plastic zone near the crack is shown in Figs. 5.25a, 5.25b

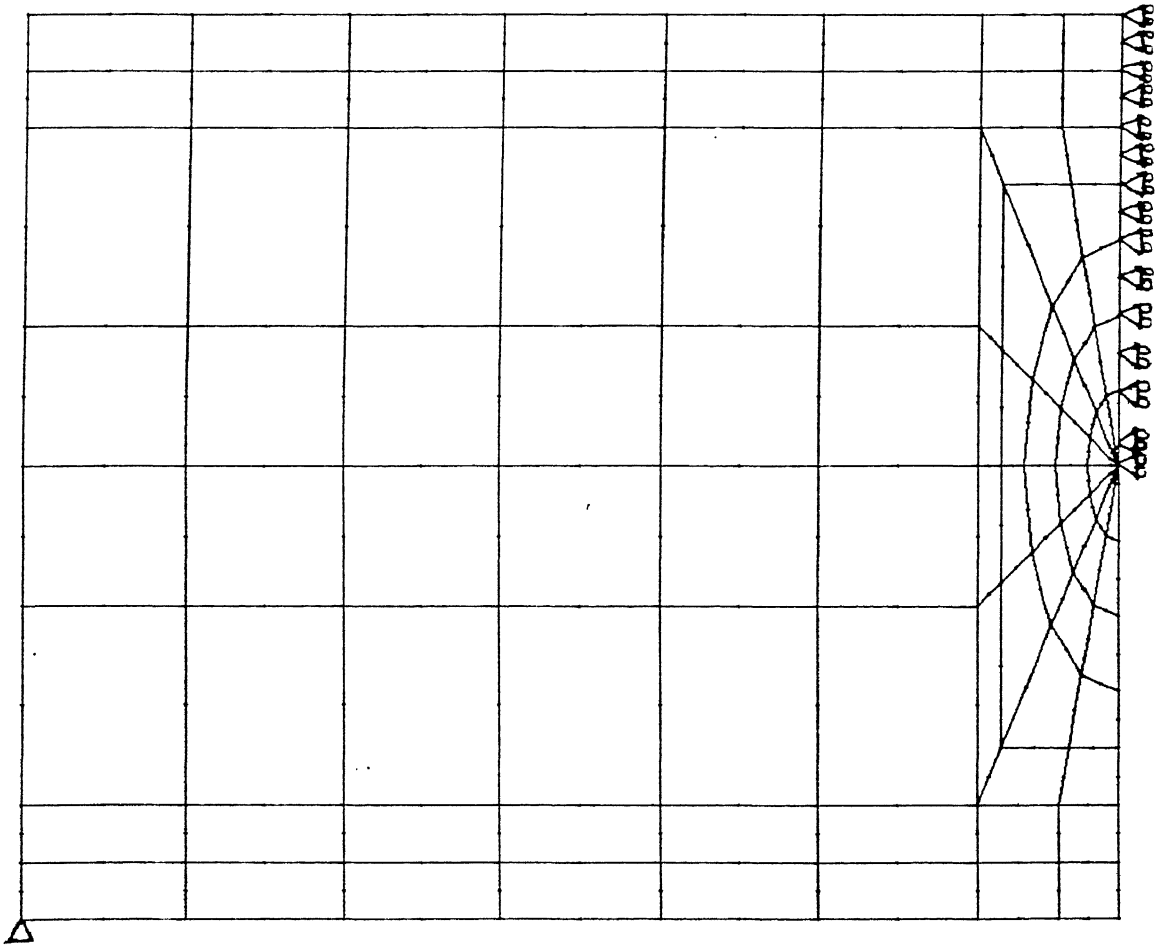

Figure 5.11: Finite element mesh for the cracked beam

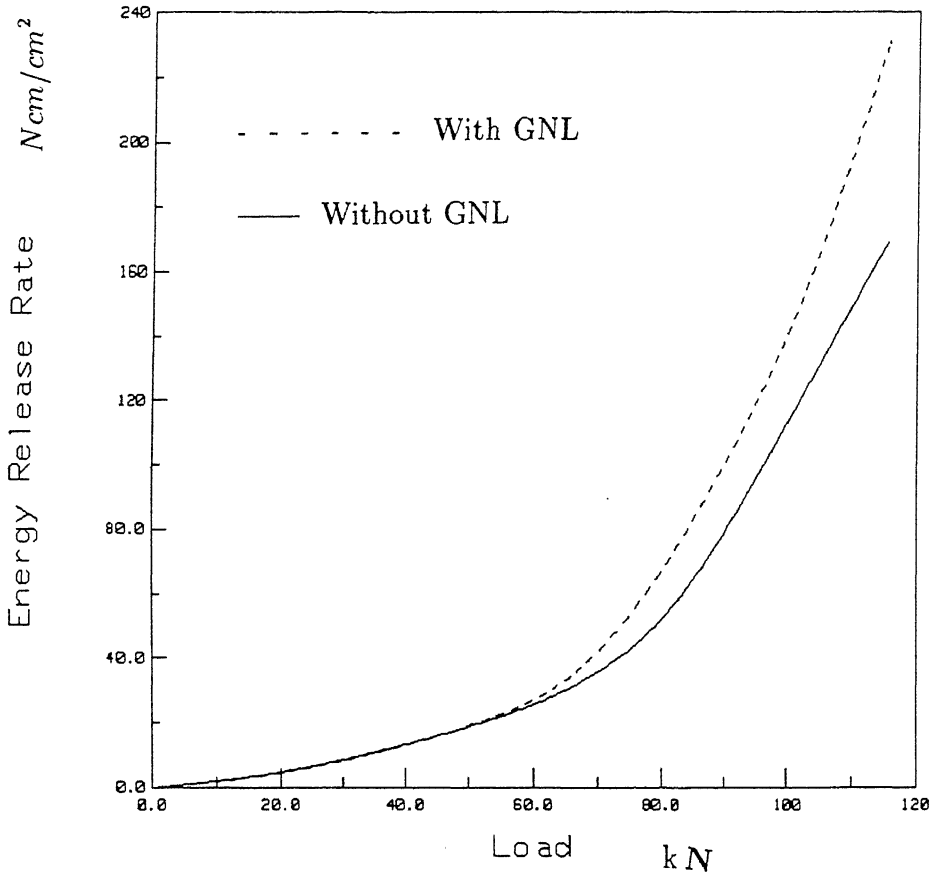

Figure 5.12: Energy Release Rate vs Load for cracked beam

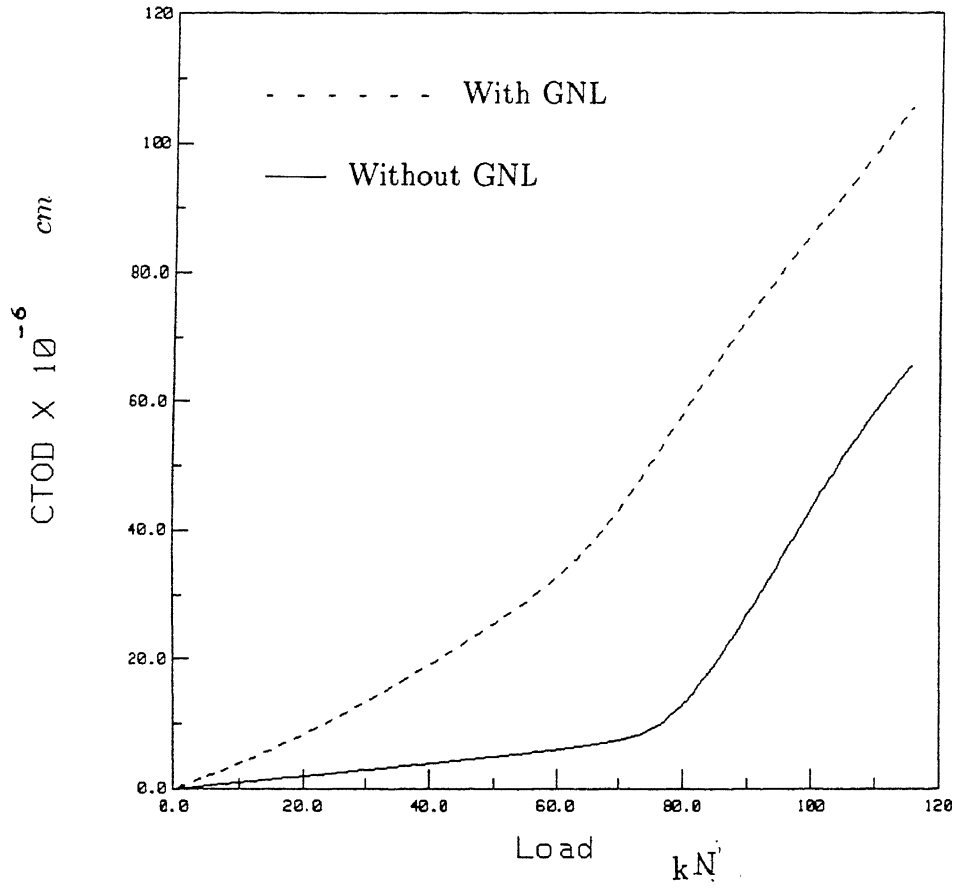

Figure 5.13: CTOD vs Load for cracked beam

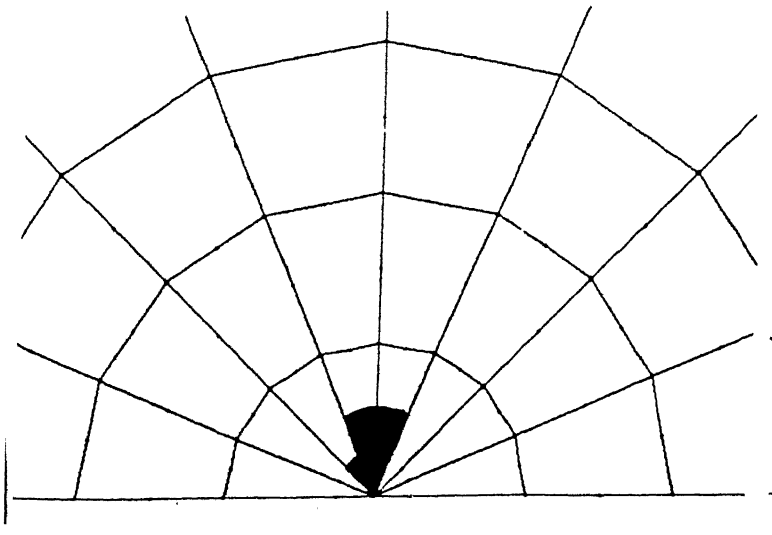

a) $P = 69.3$

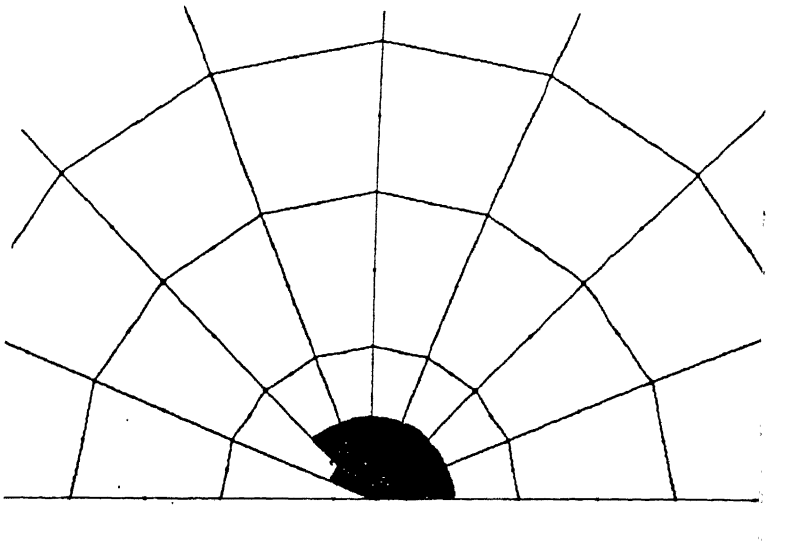

b) $P = 92.4$

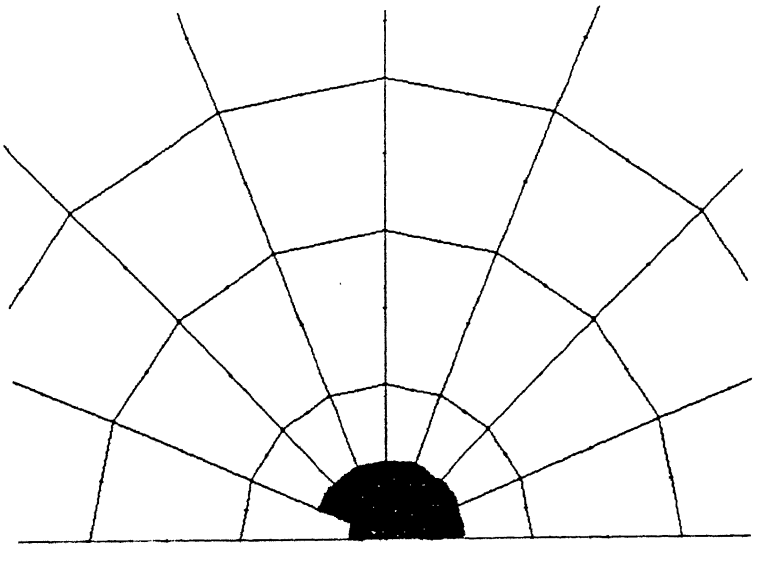

c) $P = 115$

Figure 5.14: Spread of Plastic zone for cracked beam

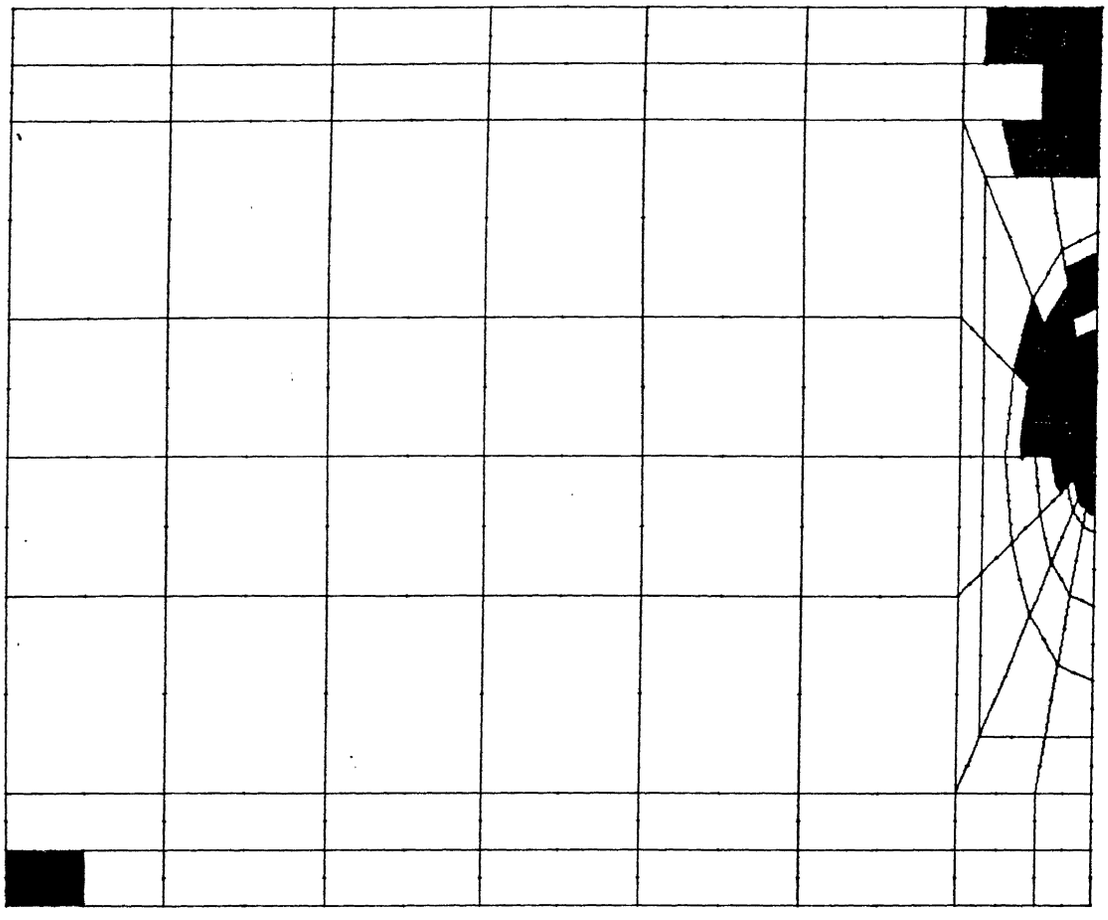

Figure 5.15: Spread of Plastic zone for cracked beam at limit load

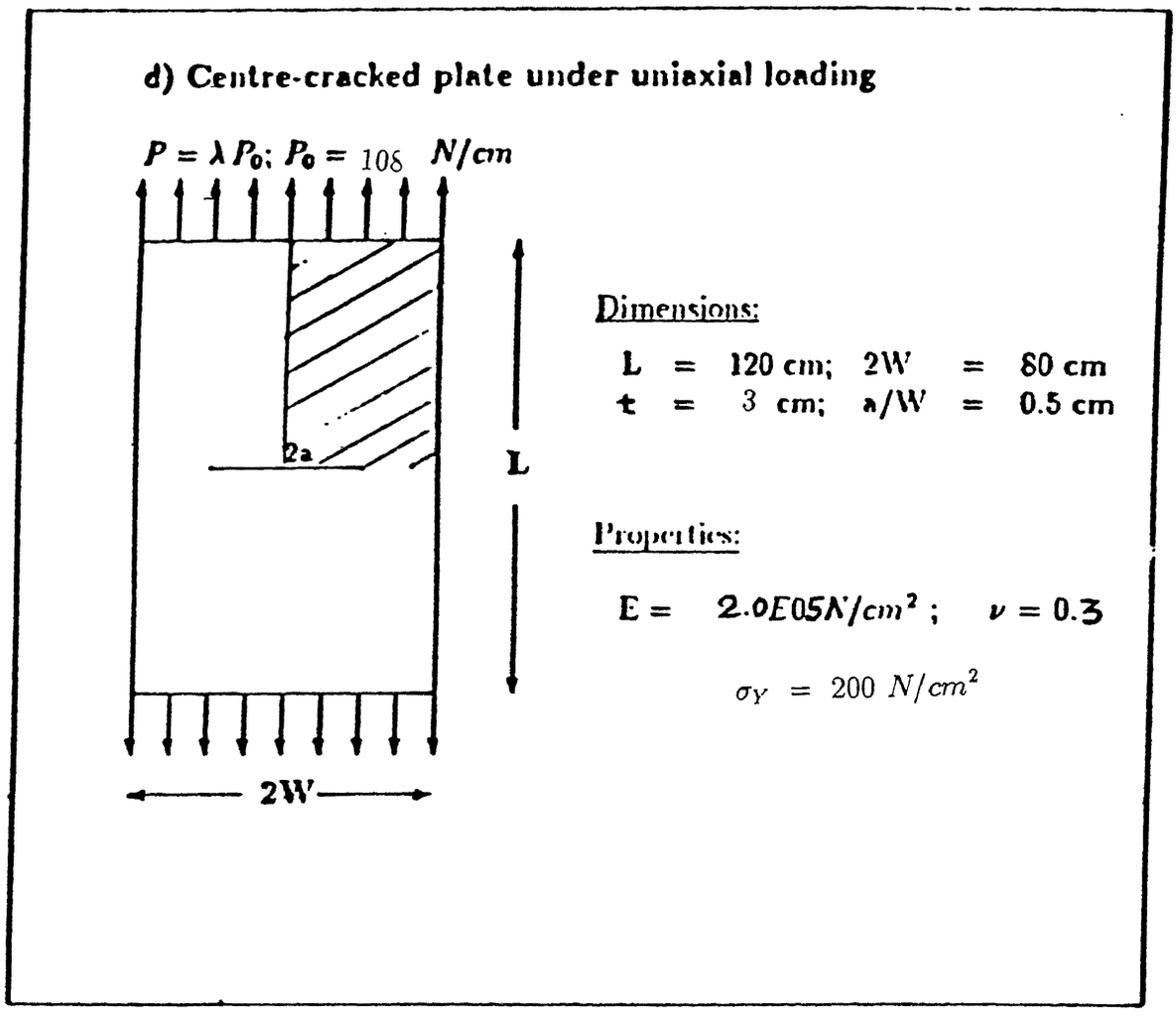

Figure 5.16: Center-cracked plate under uniaxial loading

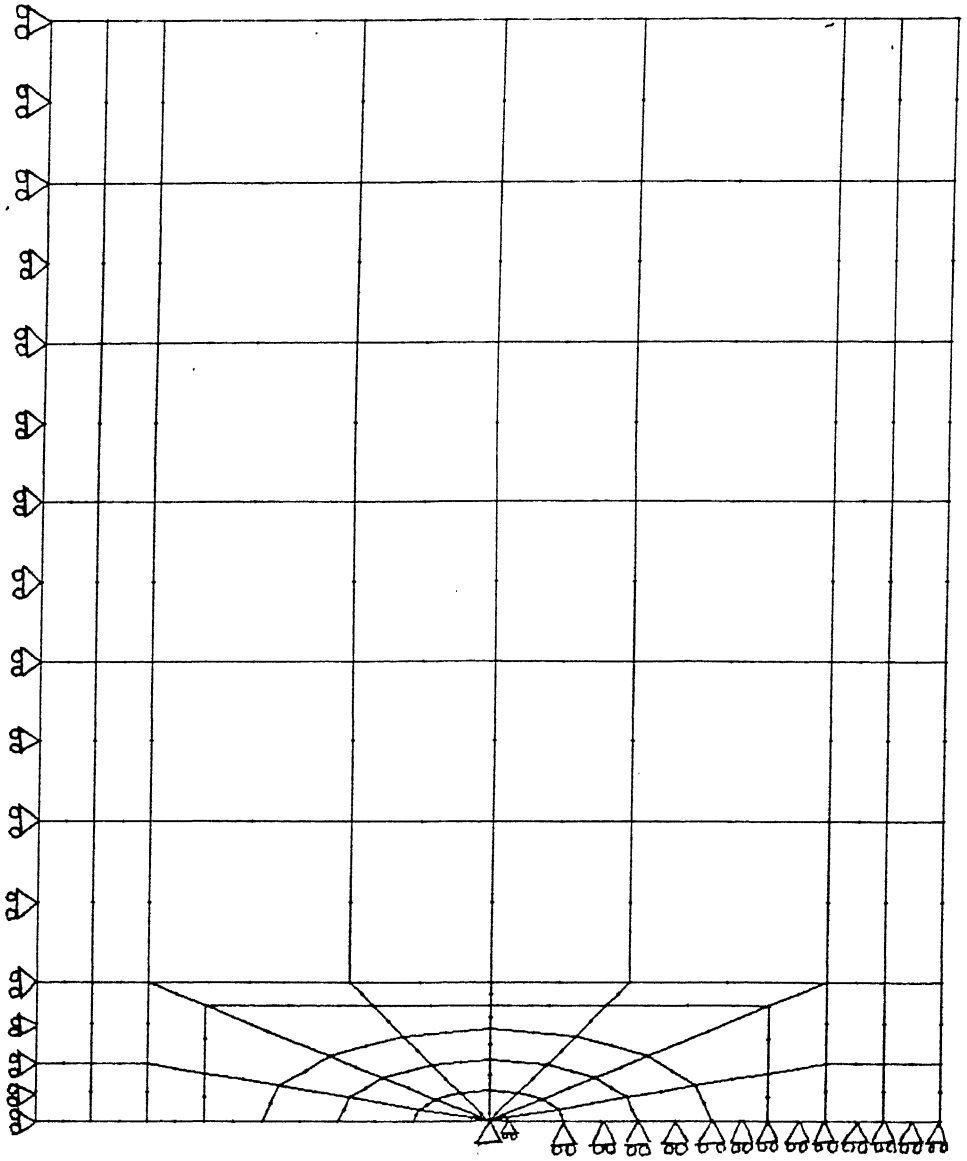

Figure 5.17: Finite element mesh for the center-cracked plate

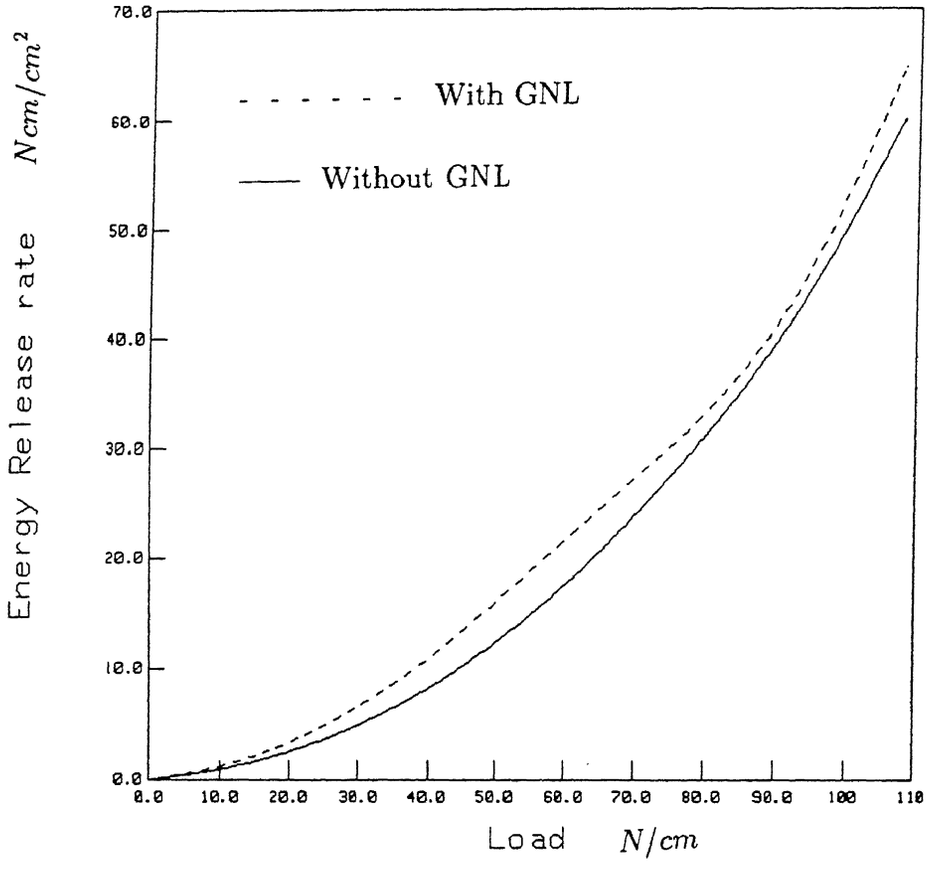

Figure 5.18: Energy Release Rate vs Load for center-cracked plate

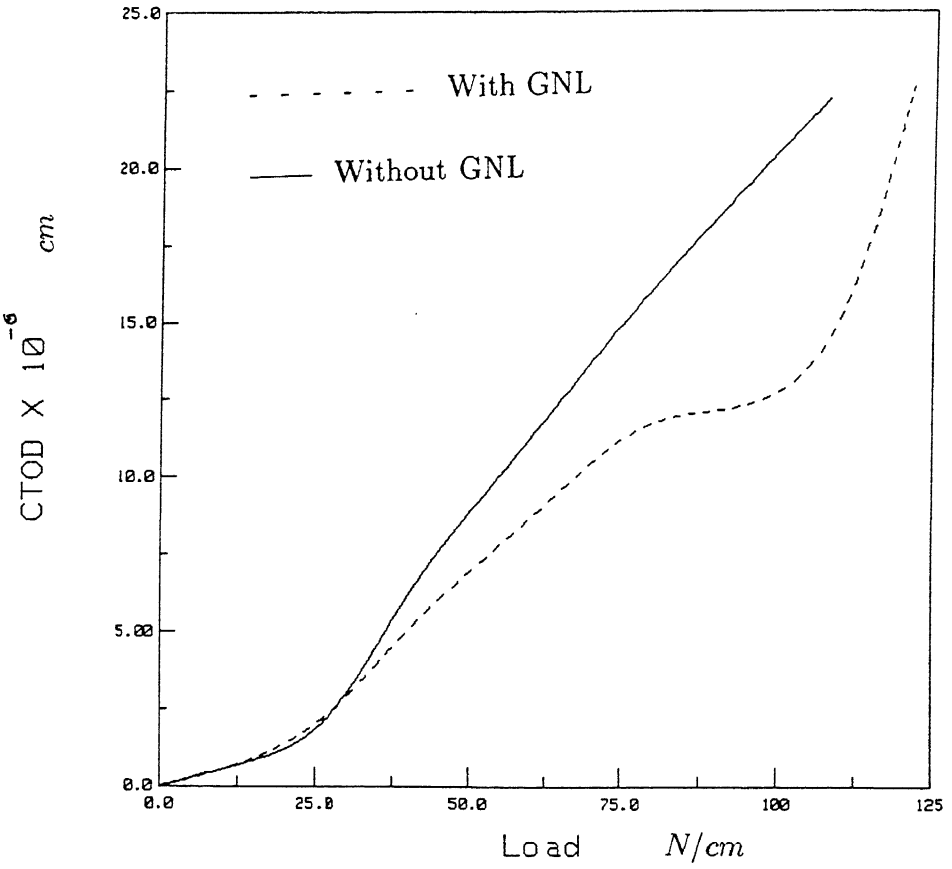

Figure 5.19: CTOD vs Load for center-cracked plate

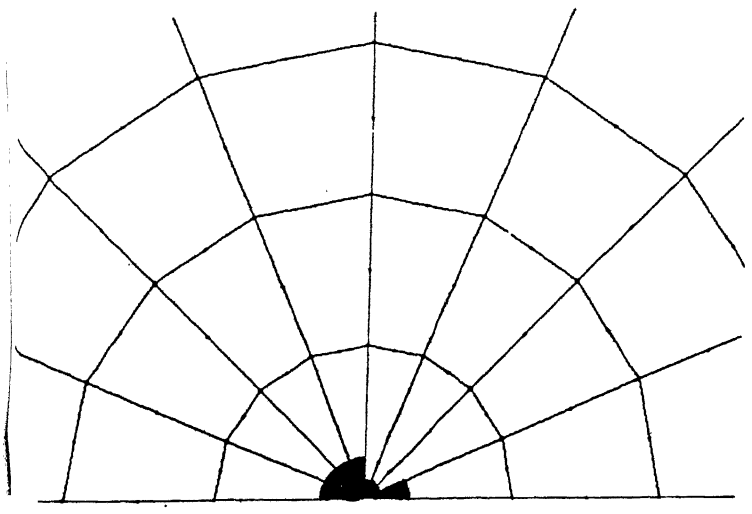

a) $P = 40.5$

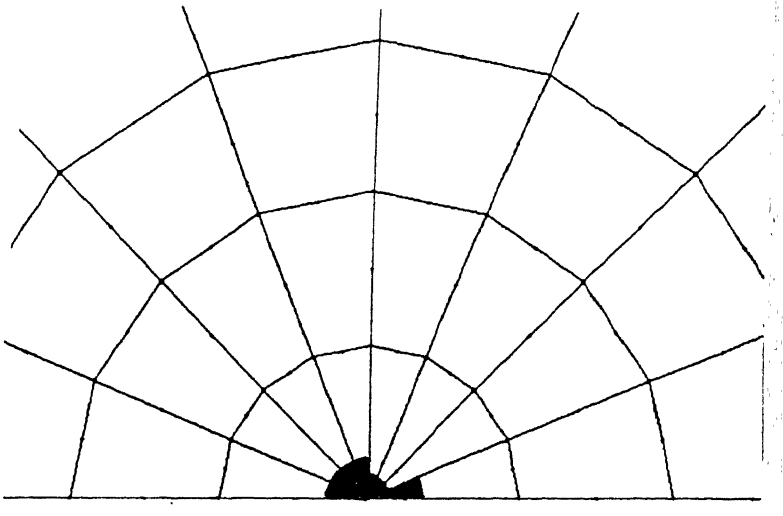

b) $P = 67.5$

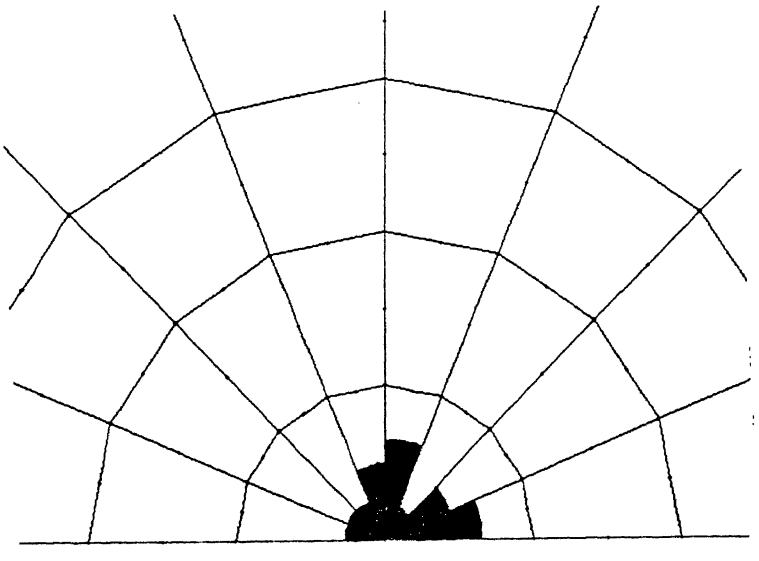

c) $P = 108$

Figure 5.20: Spread of Plastic zone for center-cracked plate

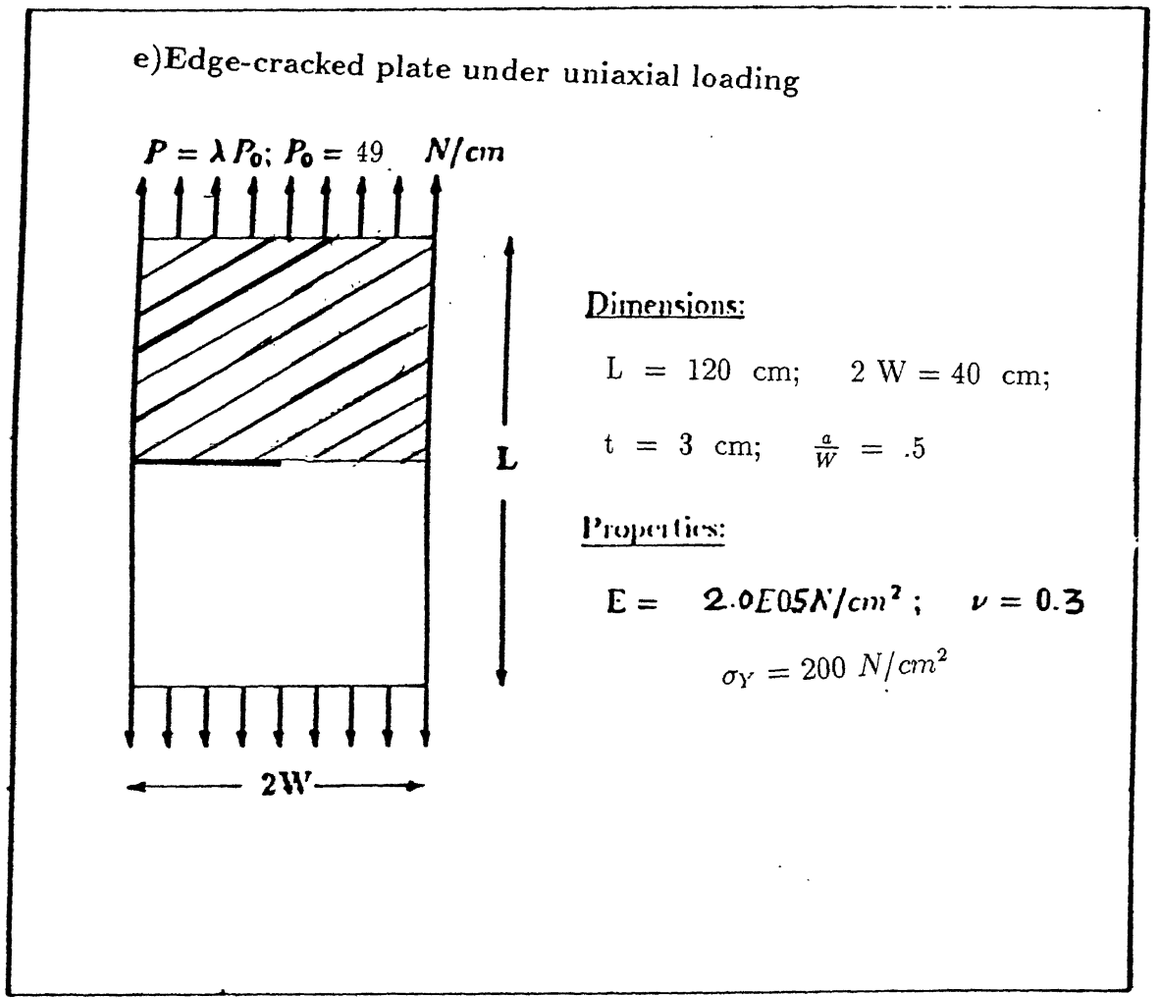

Figure 5.21: Edge-cracked plate under uniaxial loading

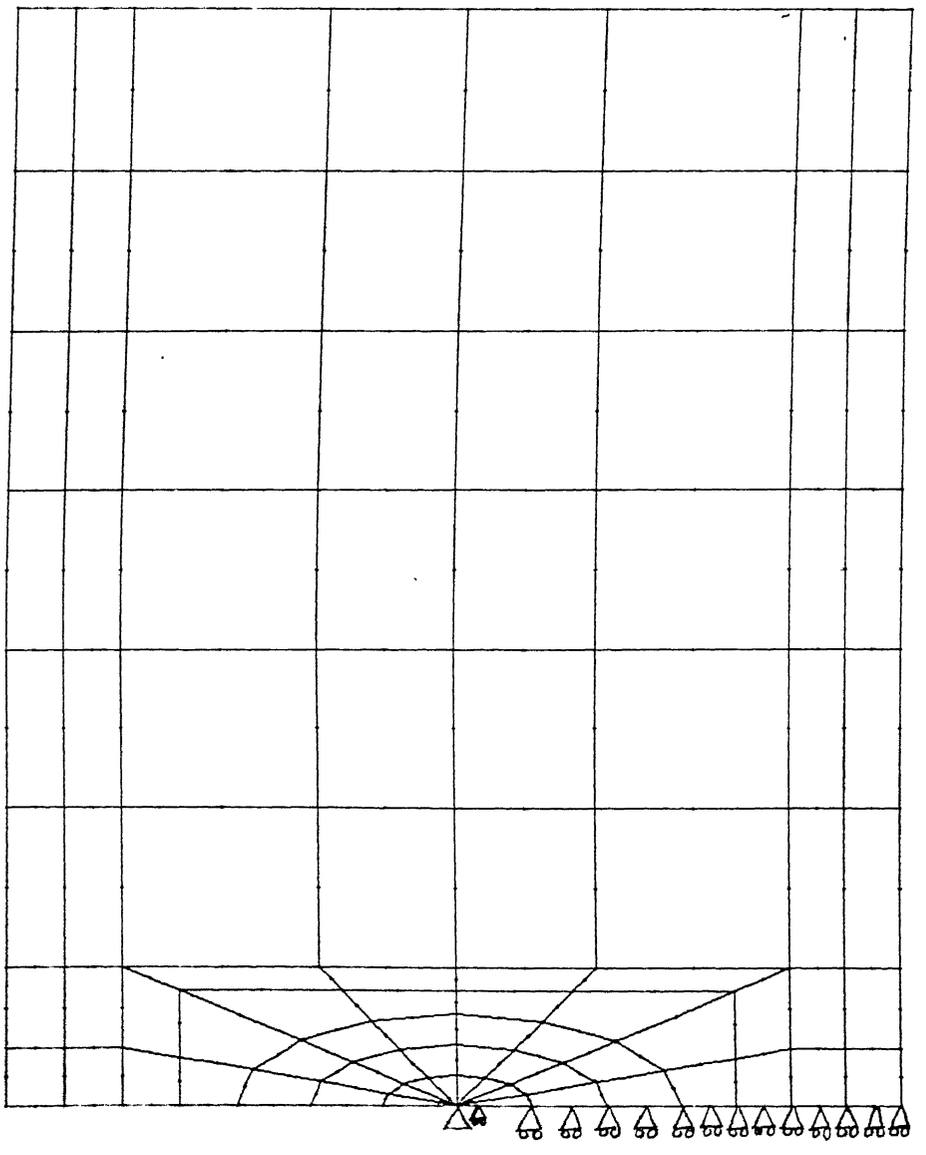

Figure 5.22: Finite element mesh for the Edge-cracked plate

and 5.25c.

Cracked Bodies with Elastic Linearly Strain Hardening Material

The problems of simply supported beam with a central crack, plate with center crack and plate with edge crack are solved in this section assuming that the material is elastic and linearly strain hardening in nature. The strain hardening co-efficient is taken to be $H' = 2X10^4$.

The effect of geometric nonlinearity on energy release rate and CTOD for simply supported beam with central crack is shown in Figs. 5.26 and 5.27. The plastic zone near the crack is shown in Figs. 5.28a, 5.28b and 5.28c.

The effect of geometric nonlinearity on energy release rate and CTOD for plate with center crack is shown in Figs. 5.29 and 5.30. The plastic zone near the crack is shown in Figs. 5.31a, 5.31b and 5.31c.

The effect of geometric nonlinearity on energy release rate and CTOD for plate with edge crack is shown in Figs. 5.32 and 5.33. The plastic zone near the crack is shown in Figs. 5.34a, 5.34b and 5.34c.

It is observed that for same load the body with elastic perfectly plastic material has higher energy release rate and larger CTOD than the body with elastic linearly strain hardening material.

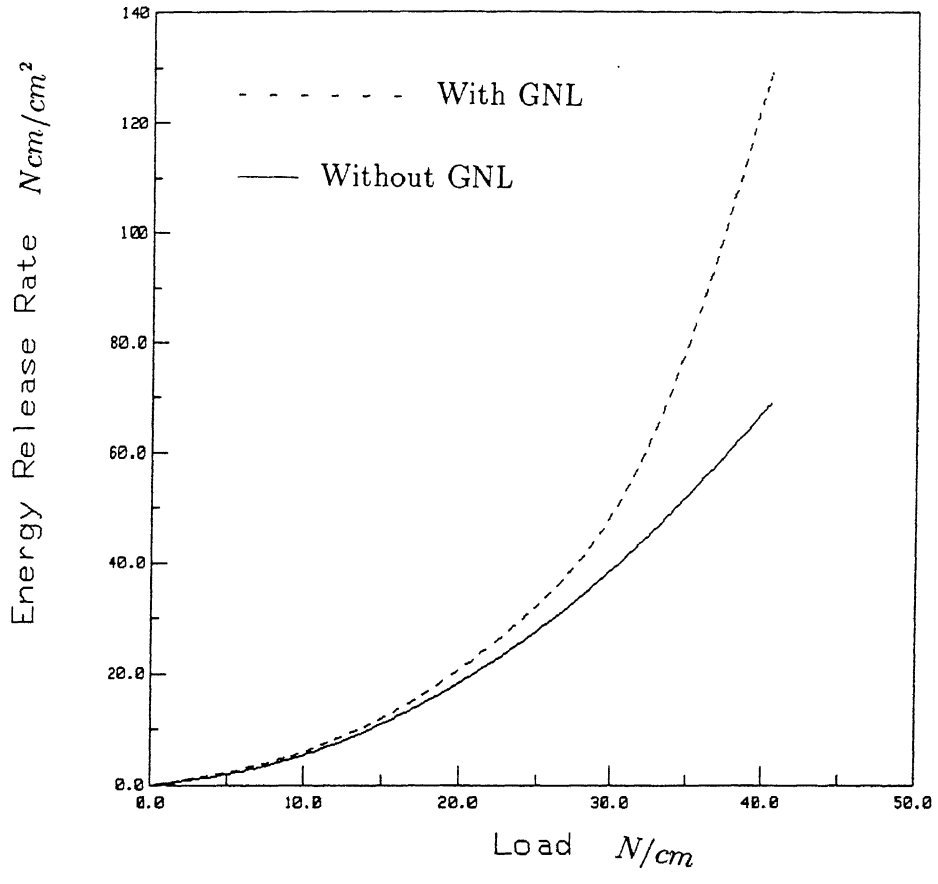

Figure 5.23: Energy Release Rate vs Load for Edge-cracked plate

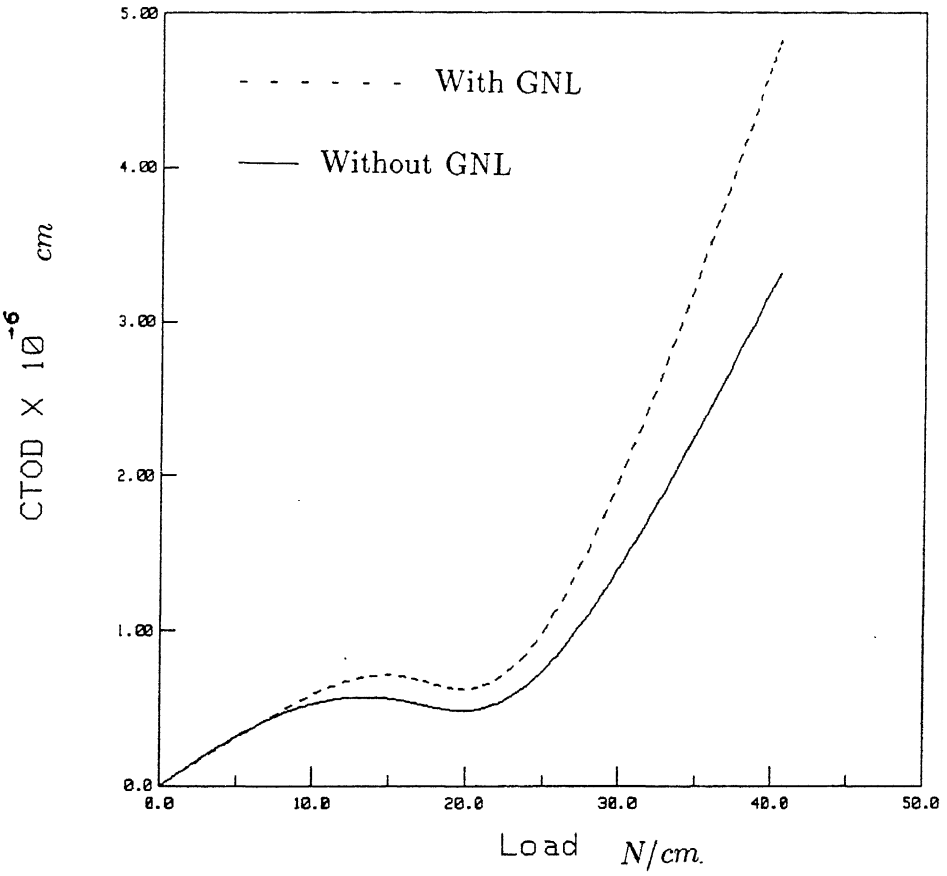

Material : Elastic Perfectly Plastic

Figure 5.24: CTOD vs Load for Edge-cracked plate

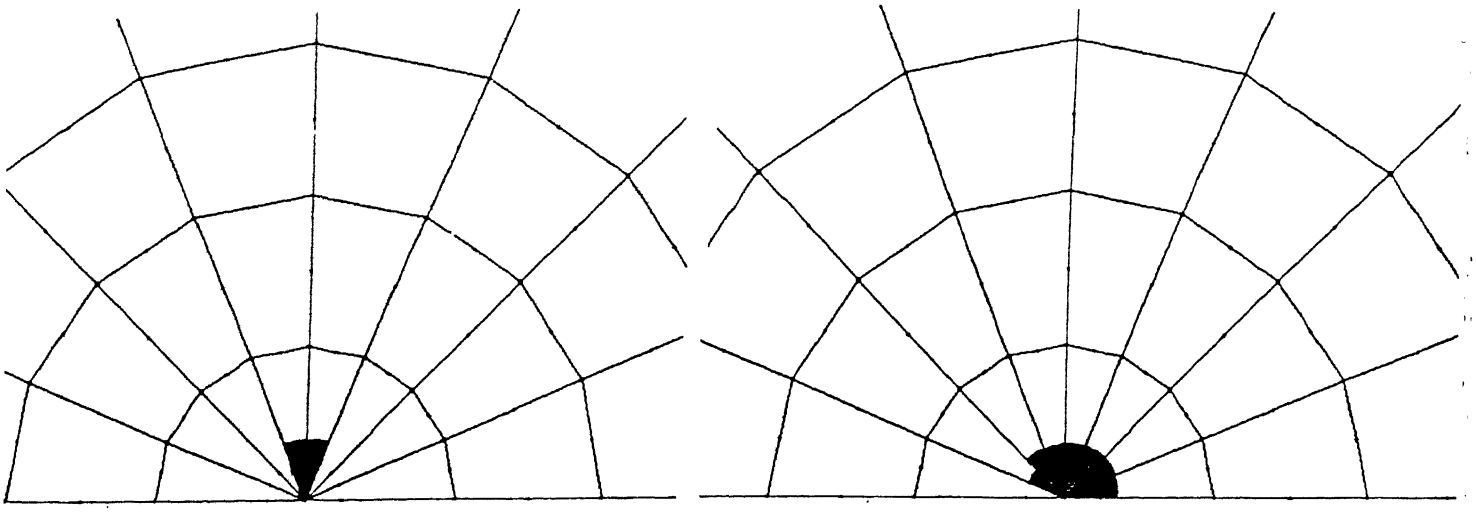

a) $P = 16.2$ *b*) $P = 32.4$

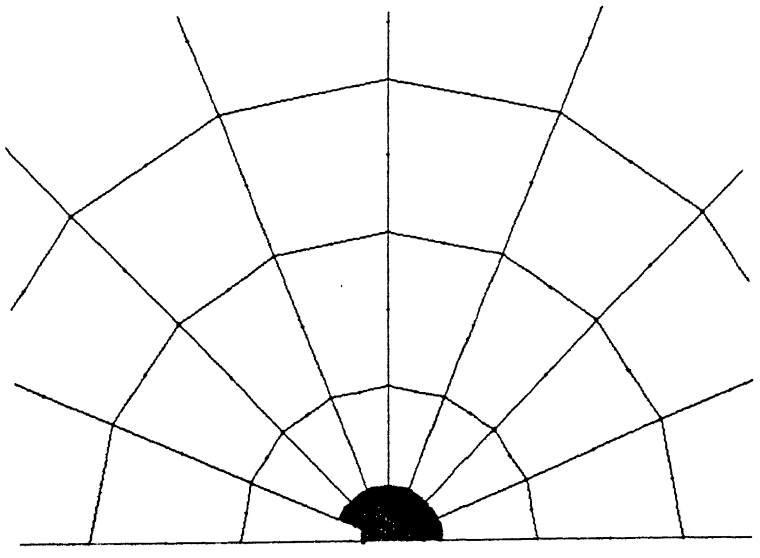

c) $P = 40.5$

Figure 5.25: Spread of Plastic zone for Edge-cracked plate

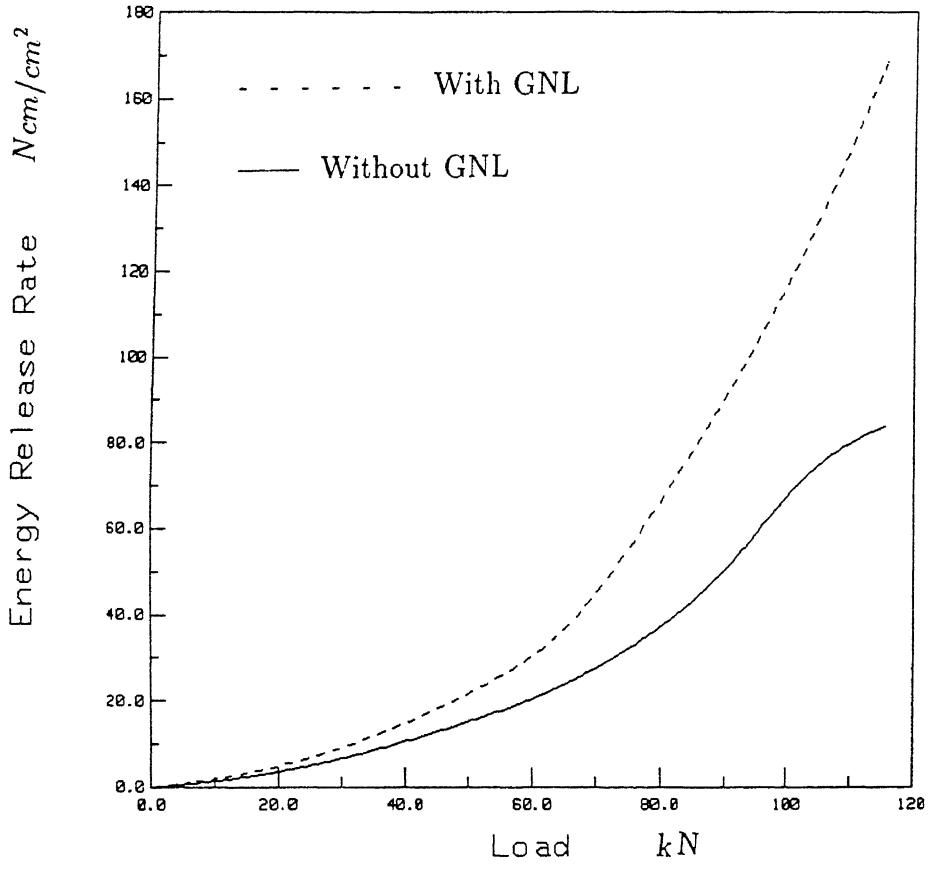

Figure 5.26: Energy Release Rate vs Load for cracked beam

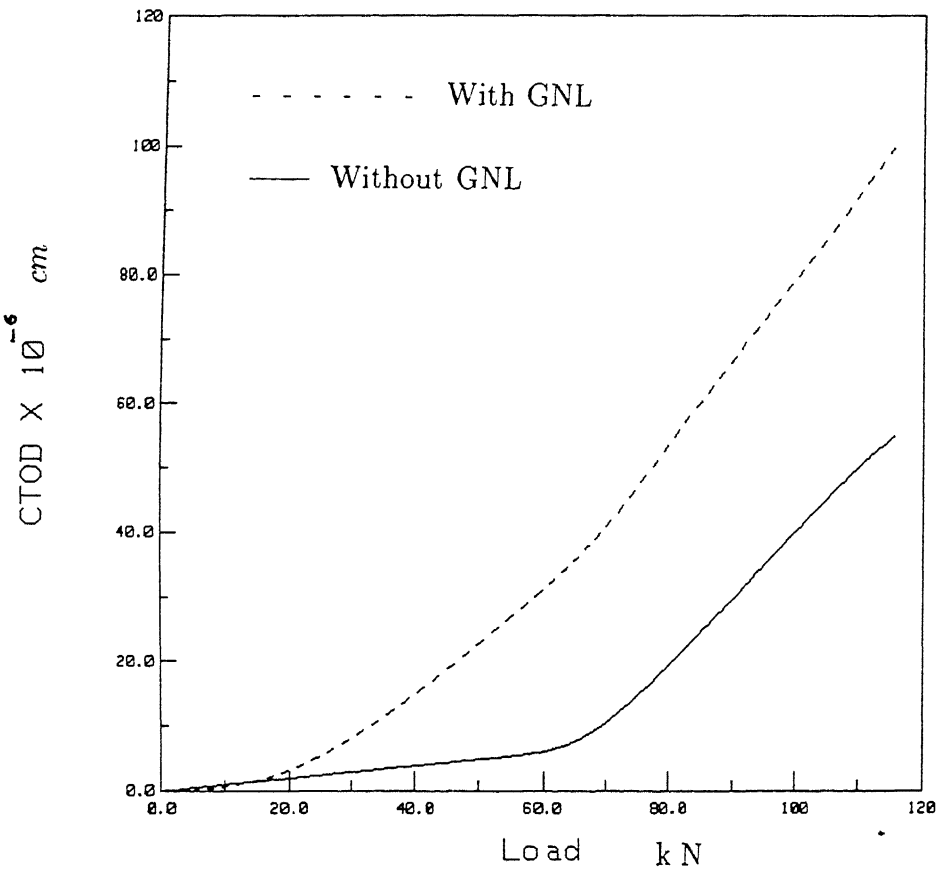

Figure 5.27: CTOD vs Load for cracked beam

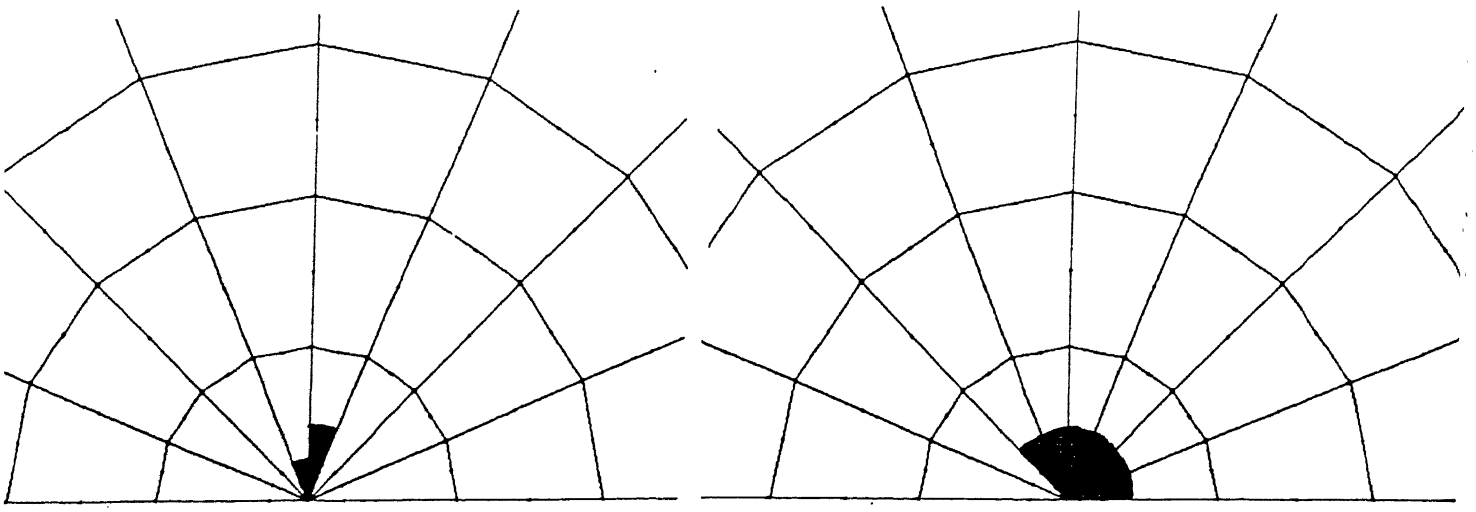

a) $P = 57.75$ *b*) $P = 80.85$

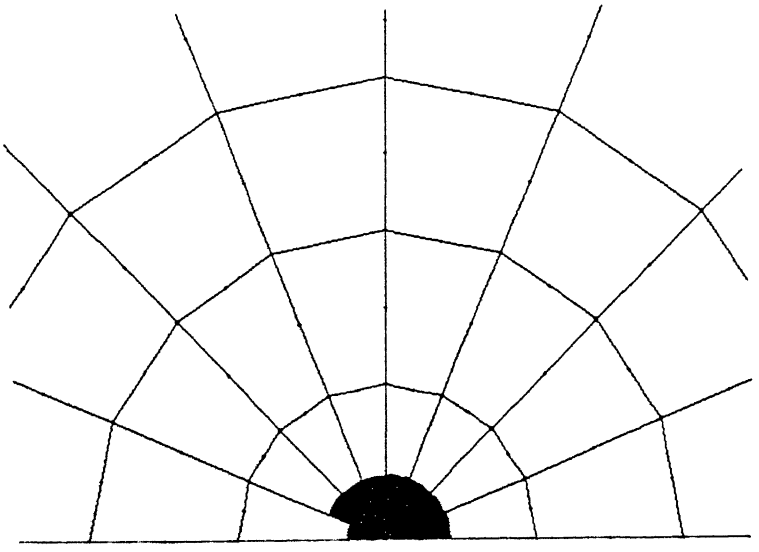

c) $P = 115$

Figure 5.28: Spread of Plastic zone for cracked beam

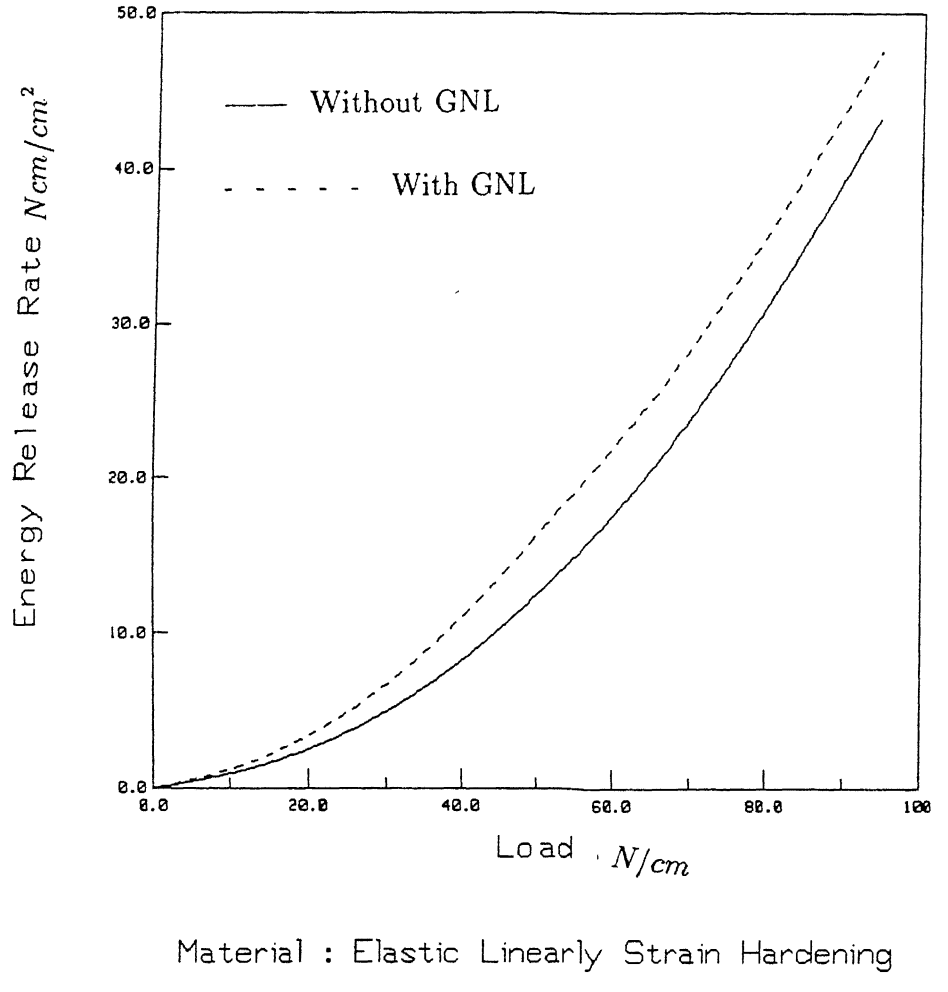

Figure 5.29: Energy Release Rate vs Load for center-cracked plate

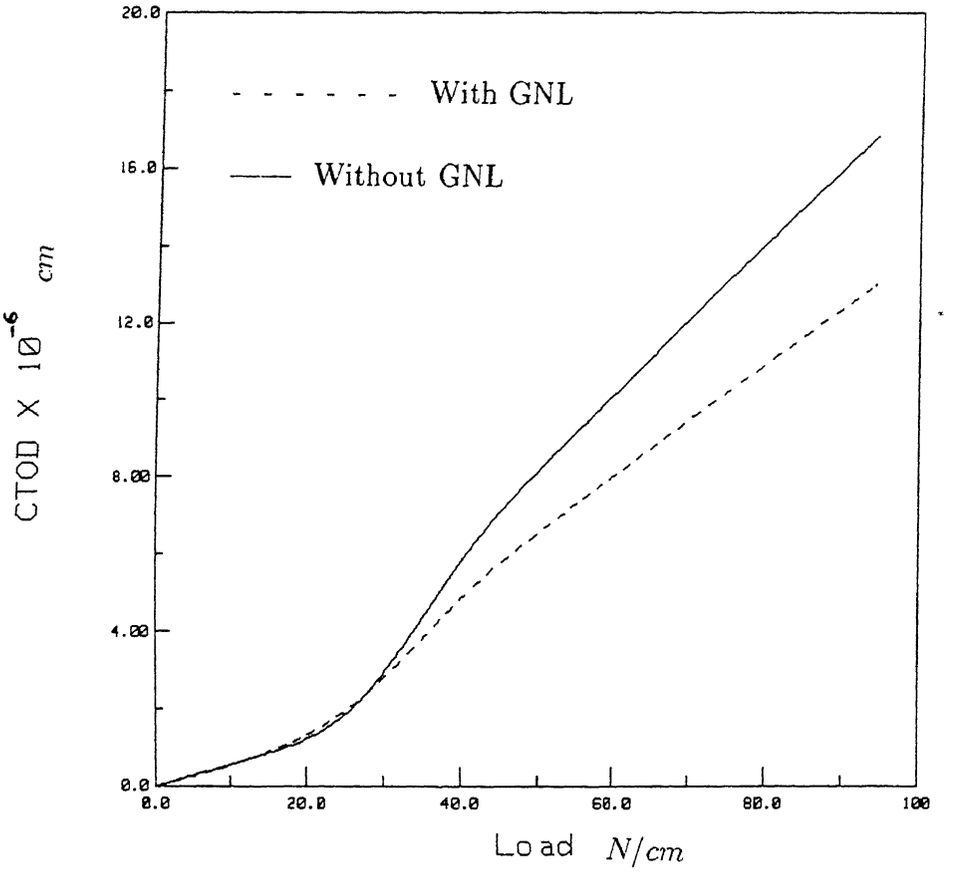

Figure 5.30: CTOD vs Load for center-cracked plate

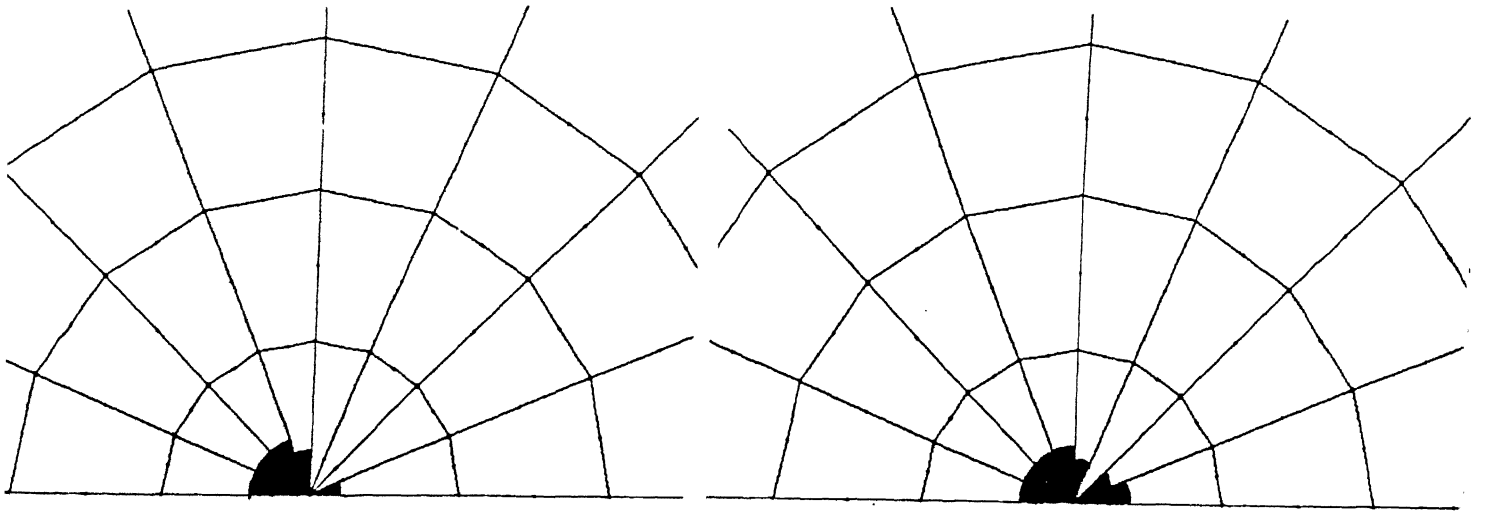

a) $P = 27$ *b*) $P = 54$

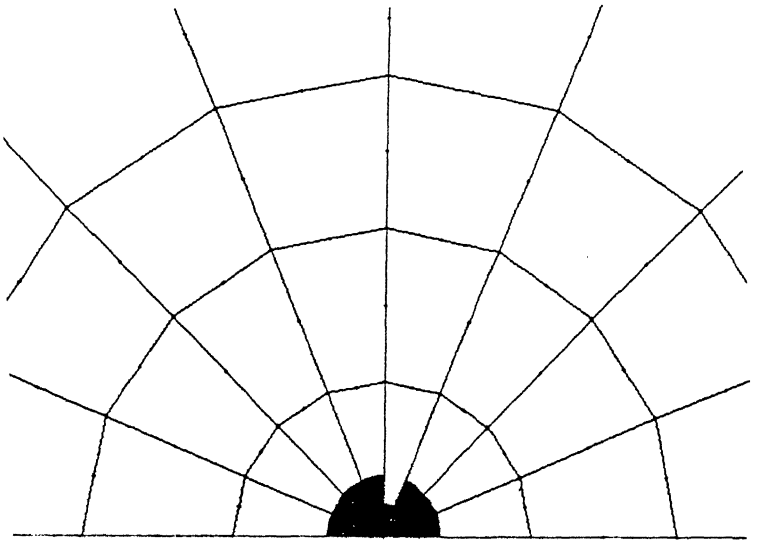

c) $P = 94.5$

Figure 5.31: Spread of Plastic zone for center-cracked plate

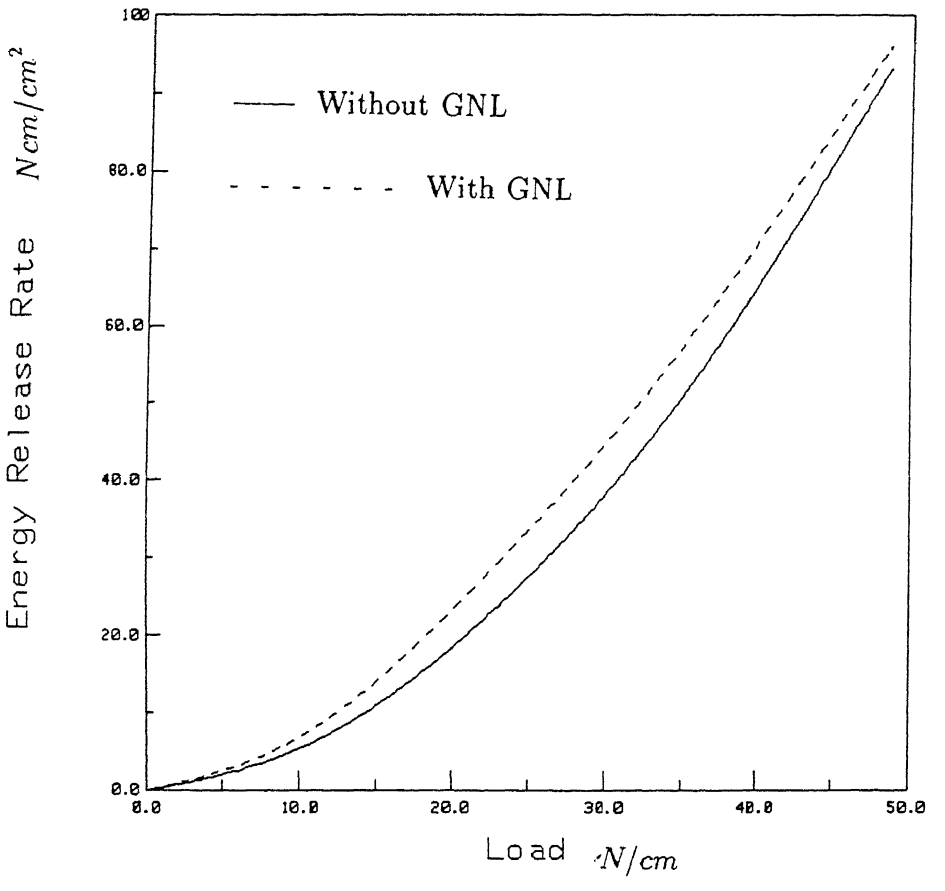

Figure 5.32: Energy Release Rate vs Load for edge-cracked plate

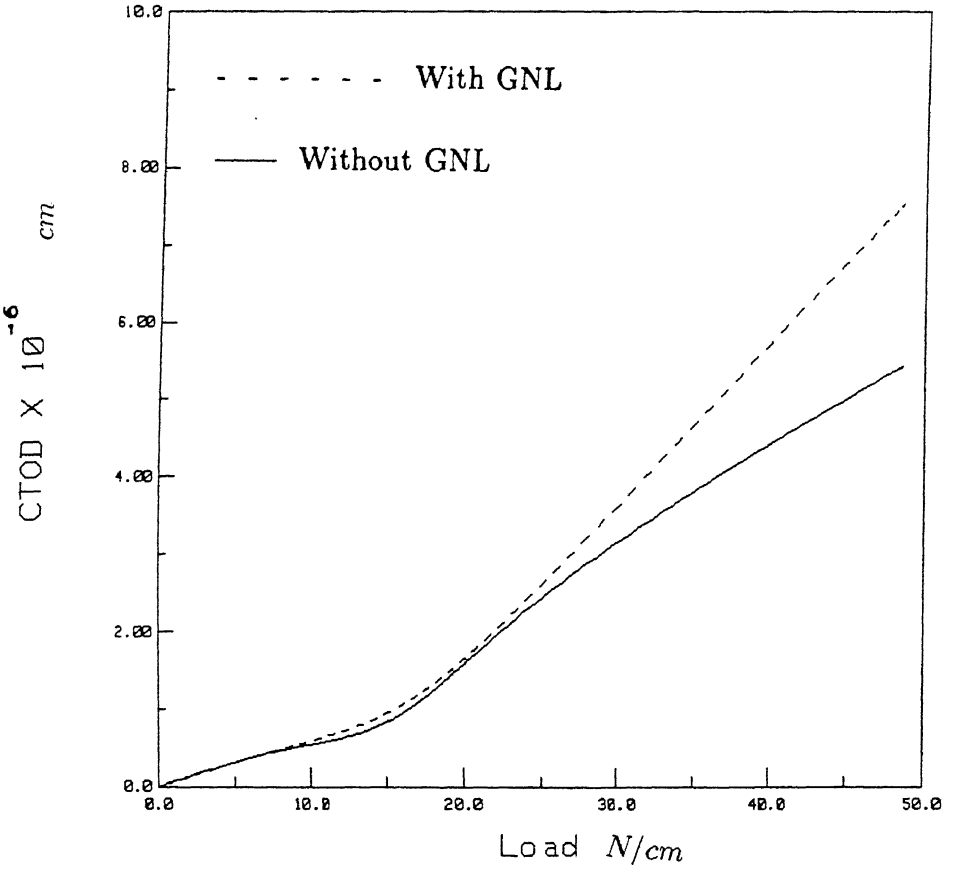

Figure 5.33: CTOD vs Load for edge-cracked plate

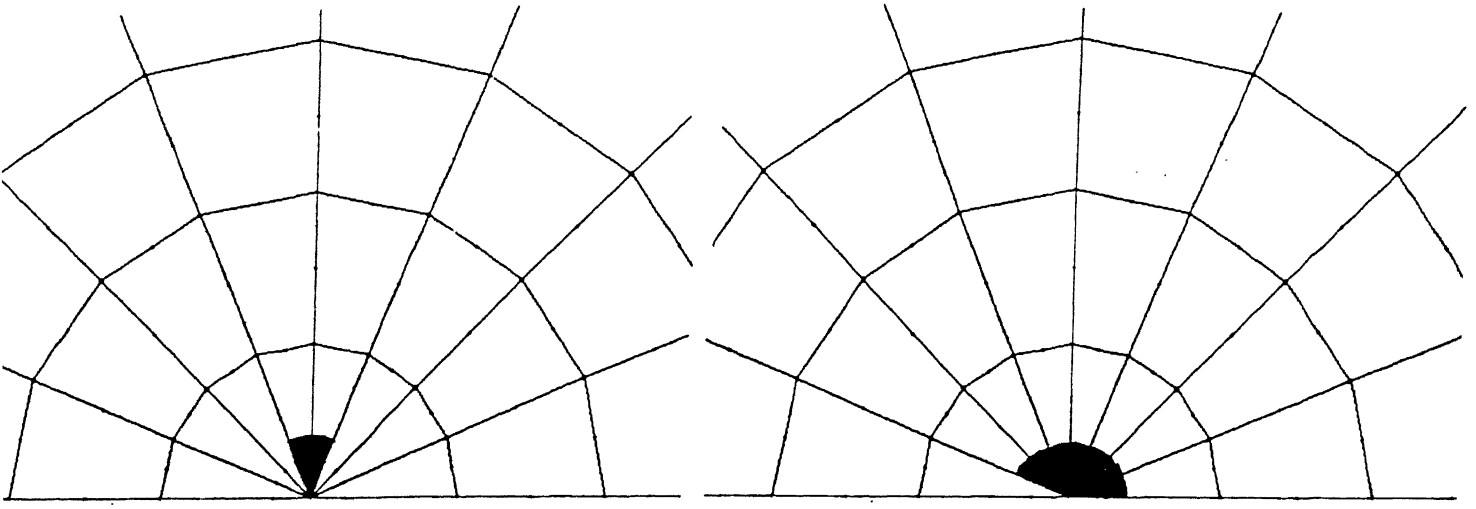

a) $P = 16.2$

b) $P = 32.4$

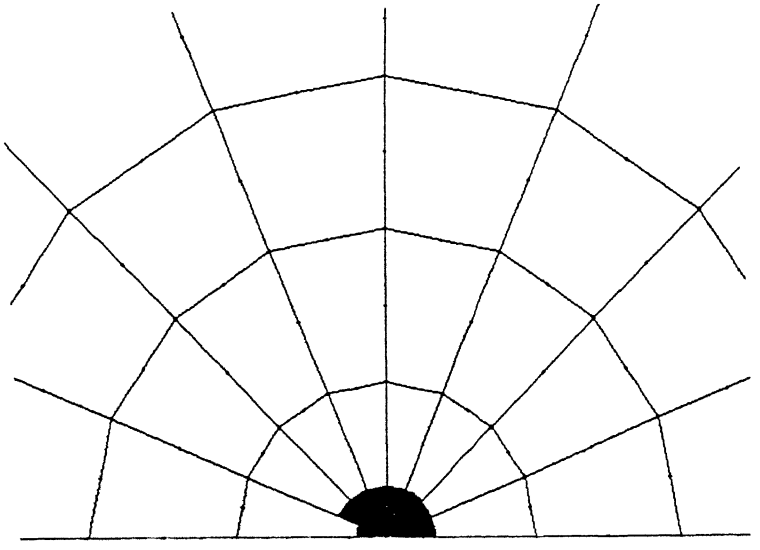

c) $P = 48.6$

Figure 5.34: Spread of Plastic zone for edge-cracked plate

Chapter 6

CONCLUSIONS AND SCOPE FOR FUTURE WORK

The following conclusions can be drawn from the present study

- Geometric and Material nonlinearities have been successfully modelled.
- The nonlinearity due to large deformations in the structure influences the load displacement characteristic to a great extent.
- Geometric nonlinearity has influence on the fracture parameters. Therefore to have a more accurate design Geometric nonlinearity should be considered in evaluating fracture parameters.

Scope For Future Work

- Modified Newton raphson technique takes significant time as we go for mesh refinement in our analysis. Inclusion of some acceleration scheme in this method would make the program computationally more efficient.
- Present work can be extended to include the dynamic analysis of cracked structures thus making it more general.

References

1. kawai,T. and Yoshimura, N. - Analysis of large deflection of plates by the finite element method, Int. J. Num. Meth. Engng., Vol. 1, pp. 123-133, 1969.

2. Bergan, P.G. and Clough, R.W. - Large deflection analysis of plates and shallow shells using the finite element method, Int. J. Num. Meth. Engng., Vol 5, pp. 543-556, 1973.

3. Bathe, K.J. and Ozdemir, H. - Elastic-Plastic large deformation static and dynamic analysis, Computers and Structures, vol. 6, pp. 81-92, 1976.

4. Bathe, K.J. and Bolourchi, S. - Large displacement analysis of Three - dimensional beam structures, Int. J. Num. Meth. Engng., Vol. 14, pp. 961-986, 1979.

5. Oden, J.T. - Finite Elements of Nonlinear Continua, McGraw Hill, New York, 1972.

6. Hibbit, H.D., Marcal, P.V. and Rice, J.R. - A Finite Element formulation for problems of large strain and large displacements, Int. J. Solids and Struct., Vol. 6, pp. 1069-1086, 1970.

7. Turner, M.J., Dill, E.H., Martin, H.C. and Melosh, R.J. - Large deflection analysis of complex structures subjected to heating and external loads, J. Aero. Sci., Vol. 27, pp. 97-106, 1960.

8. Argyris, J.H., Kelsey, S. and Kamel, H. - Matrix methods of structural analysis, pp. 105-120, Pergamon Press, 1964.

9. Gallagher, R.H., Gellaty, R.A., Padlog, J. and Mallett, R.H. - Discrete element procedure for thin shell instability analysis, AIAA Jnl., Vol. 5, pp. 138-144, 1967.

10. Zienkiewicz, O.C. - The finite element method in structural and continuum mechanics, McGraw Hill, 1992.

11. Yaghmai, S. and Popov, E.P. - Incremental analysis of large deflections of shells of revolution, Int. J. Solids and Struct., Vol. 7, pp. 1375-1393, 1971.

12. Stricklin, J.A., Von Riesemann, W.A., Tillerson, J.R. and Haisler, W.E. - Static geometric and material nonlinear analysis, Advances in computational methods in structural mechanics and design, 2nd U.S.-Japan Seminar Matrix Meth. Struct. Analysis and Design, Univ. of Alabama Press, pp. 301-324, 1972.

13. McMeeking, R.M. and Rice, J.R. - Finite element formulations for large elastic plastic deformations, Int. J. Solids and Struct., Vol. 11, pp. 601-616, 1975.

14. Cook, R.D., Malkus,D.S. and Plesa, M.C. - Concepts and Applications of Finite Element Analysis, John Wiley ans Sons, 1989.

15. Bathe, K.J., Ramm, E. and Wilson, E.L. - Finite element formulations for large deformation dynamic analysis, Int. J. Num. Meth. Engng., Vol. 9, pp. 353-386, 1975.

16. Barsoum, R.S. - Application of quadratic isoparametric finite elements in linear fracture mechanics, Int. J. Fract., Vol. 10, pp. 603-605, 1974.

17. Barsoum, R.S. - Further application of quadratic isoparametric finite elements to linear fracture mechanics of plate bending and general shells, Int. J. Fract., Vol. 11, pp. 167-169, 1975.

18. Barsoum, R.S. - On the use of isoparametric finite elements in linear fracture mechanics, Int. J. Num. Meth. Engng., Vol. 10, pp. 25-37, 1976.

19. Barsoum, R.S. - A degenerate solid element for linear fracture analysis of plate bending and general shells, Int. J. Num. Meth. Engng., Vol. 10, pp. 551-564, 1976.

20. Alwar, R.S. and Thiagarajan, S. - Combined effect of shear and large deformation on stress intensity factors, Int. J. Num. Meth. Engng., Vol. 28, pp. 1951-1964, 1989.

21. Atluri, S.N. and Nakagaki, M. - Stress Analysis of cracks in the elasto-plastic Range, Proceedings of the Fourth International Conference on Fracture, Waterloo, Vol. 3, pp. 457-462, 1977.

22. Bergez, D., Nguyen, Q. S. and Radenkovic, D. - Elastic-plastic analysis of crack opening and crack closure, Numerical Methods in Fracture Mechanics., pp. 327-342, 1980.

23. Roche, R.L. - Use of calculation of J Integral, Proceedings of the Fourth International Conference on Fracture, Waterloo, Vol. 3, pp. 247-256, 1977.

24. Albert S. Kuo and Liu, H.W. - An experimental and FEM Study on crack opening displacement, Proceedings of the Fourth International Conference on Fracture, Waterloo, Vol. 3, pp. 311-320, 1977.

25. Clarke, C.K. - Studies of crack tips in steel and Aluminium alloys, Proceedings of the Fourth International Conference on Fracture, Waterloo, Vol. 3, pp. 321-328, 1977.

26. Barsoum, R.S. - Triangular quarter point elements as elastic and perfectly plastic crack tip elements, Int. J. Num. Meth. Engng., Vol. 2, pp. 85-90, 1977.

27. Bathe, K.J. - Finite element procedures in Engng. analysis, Prentice - Hall of India, New Delhi, 1990.

28. Bridgman, P.W. - Studies in large plastic flow and fracture, McGraw Hill, New York, 1952.

29. Hill, R. - The Mathematical Theory of Plasticity, Oxford Univ. Press, 1950.

30. Hinton, E. and Owen, D.R.J., Finite elements in plasticity, Pinridge Press Limited, Swansea, U.K, 1980.

31. Nayak, G.C. and Zienkiewicz, O.C. - Convinient form of stress invariants for plasticity, Journal of the struct. Div. Proc. of ASCE., pp. 949-953, April 1972.

32. Owen, D.R.J. and Fawkes, A.J. - Engineering Fracture Mechanics : Numerical methods and applications, Pineridge Press Ltd., Swansea, U.K.

33. Rice, J.R. - A path independent integral and the approximate analysis of strain concentration by notches and cracks, J. App. Mech., pp. 379-386, 1968.

34. Saje, M. and srpcic, S. - Large deformations of in-plane beam, Int. J. Solids and Struct., Vol. 21, pp. 1181-1195, 1985.

35. Raghu Raman, R. - Finite Element Modelling of Geometric Nonlinearity and study of Fracture Problems, M.Tech. Thesis, Department of Mechanical Engineering, IIT Kanpur, India.

Appendix

Matrices used in two dimensional analysis in T.L formulation

Incremental Strains

$$
\begin{aligned}
{}_0\epsilon_{11} &= {}_0u_{1,1} + {}^t_0u_{1,1}\ {}_0u_{1,1} + {}^t_0u_{2,1}\ {}_0u_{2,1} + \frac{1}{2}(({}_0u_{1,1})^2 + ({}_0u_{2,1})^2) \\
{}_0\epsilon_{22} &= {}_0u_{2,2} + {}^t_0u_{1,2}\ {}_0u_{1,2} + {}^t_0u_{2,2}\ {}_0u_{2,2} + \frac{1}{2}(({}_0u_{1,2})^2 + ({}_0u_{2,2})^2) \\
{}_0\epsilon_{12} &= \frac{1}{2}({}_0u_{1,2} + {}_0u_{2,1}) + \frac{1}{2}({}^t_0u_{1,1}\ {}_0u_{1,2} + {}^t_0u_{2,1}\ {}_0u_{2,2} + {}^t_0u_{1,2}\ {}_0u_{1,1} + {}^t_0u_{2,2}\ {}_0u_{2,1}) \\
&\quad + \frac{1}{2}({}_0u_{1,1}\ {}_0u_{1,2} + {}_0u_{2,1}\ {}_0u_{2,2})
\end{aligned}
$$

where ${}_0u_{i,j} = \frac{\partial u_i}{\partial {}^0x_j}$; ${}^t_0u_{i,j} = \frac{\partial {}^tu_i}{\partial {}^0x_j}$;

Linear Strain-Displacement Transformation Matrix

using ${}_0e = {}^t_0B_L\ \tilde{u}$

where ${}_0e^T = [{}_0e_{11}\ {}_0e_{22}\ 2{}_0e_{12}]$

$\tilde{u}^T = [u^1_1\ u^1_2\ u^2_1\ u^2_2\ \ldots\ u^N_1\ u^N_2]$

${}^t_0B_L = {}^t_0B_{L0} + {}^t_0B_{L1}$

$$
{}^t_0B_{L0} = \begin{bmatrix}
{}_0h_{1,1} & 0 & {}_0h_{2,1} & 0 & {}_0h_{3,1} & 0 & \ldots & {}_0h_{N,1} & 0 \\
0 & {}_0h_{1,2} & 0 & {}_0h_{2,2} & 0 & {}_0h_{3,2} & \ldots & 0 & {}_0h_{N,2} \\
{}_0h_{1,2} & {}_0h_{1,1} & {}_0h_{2,2} & {}_0h_{2,1} & {}_0h_{3,2} & {}_0h_{3,1} & \ldots & {}_0h_{N,2} & {}_0h_{N,1}
\end{bmatrix}
$$

where ${}_0h_{k,j} = \frac{\partial h_k}{\partial {}^0x_j}$; $u^k_j = {}^{t+\Delta t}u^k_j - {}^tu^k_j$;

${}^0\overline{x}_1 = \sum_{k=1}^{N} h_k\ {}^0x^k_1$; N = Number of nodes;

$$
{}^t_0B_{L1} = \begin{bmatrix}
l_{11}\ {}_0h_{1,1} & l_{21}\ {}_0h_{1,1} & \ldots & l_{21}\ {}_0h_{N,1} \\
l_{12}\ {}_0h_{1,2} & l_{22}\ {}_0h_{1,2} & \ldots & l_{22}\ {}_0h_{N,2} \\
A1 & A2 & \ldots & A3
\end{bmatrix}
$$

where

$$A1 = (l_{11}\ {}_0h_{1,2} + l_{12}\ {}_0h_{1,1})\ A2 = (l_{21}\ {}_0h_{1,2} + l_{22}\ {}_0h_{1,1})\ A3 = (l_{21}\ {}_0h_{N,2} + l_{22}\ {}_0h_{N,1})$$

where

$$l_{11} = \sum_{k=1}^{N} {}_0h_{k,1}\ {}^tu_1^k;\quad l_{22} = \sum_{k=1}^{N} {}_0h_{k,2}\ {}^tu_2^k;$$

$$l_{21} = \sum_{k=1}^{N} {}_0h_{k,1}\ {}^tu_2^k;\quad l_{12} = \sum_{k=1}^{N} {}_0h_{k,2}\ {}^tu_1^k;$$

N = Number of nodes;

Nonlinear Strain-Displacement Transformation matrix

$${}^t_0B_{NL} = \begin{bmatrix} {}_0h_{1,1} & 0 & {}_0h_{2,1} & 0 & {}_0h_{3,1} & 0 & \dots & {}_0h_{N,1} & 0 \\ {}_0h_{1,2} & 0 & {}_0h_{2,2} & 0 & {}_0h_{3,2} & 0 & \dots & {}_0h_{N,2} & 0 \\ 0 & {}_0h_{1,1} & 0 & {}_0h_{2,1} & 0 & {}_0h_{3,1} & \dots & 0 & {}_0h_{N,1} \\ 0 & {}_0h_{1,2} & 0 & {}_0h_{2,2} & 0 & {}_0h_{3,2} & \dots & 0 & {}_0h_{N,2} \end{bmatrix}$$

Second Piola-Kirchoff Stress Matrix and Vector

$${}^t_0S = \begin{bmatrix} {}^t_0S_{11} & {}^t_0S_{12} & 0 & 0 \\ {}^t_0S_{21} & {}^t_0S_{22} & 0 & 0 \\ 0 & 0 & {}^t_0S_{11} & {}^t_0S_{12} \\ 0 & 0 & {}^t_0S_{21} & {}^t_0S_{22} \end{bmatrix}$$

$${}^t_0\tilde{S}^T = [{}^t_0S_{11}\ {}^t_0S_{22}\ {}^t_0S_{12}\ ]$$

Determination of the ratio of mass densities

The mass density ratio ${}^0\rho/{}^t\rho$ can be evaluated since the mass of the particles considered is conserved:

$$\int_{{}^tV} {}^t\rho\ d^tx_1\ d^tx_2\ d^tx_3 = \int_{{}^0V} {}^0\rho\ d^0x_1\ d^0x_2\ d^0x_3$$

But

$$d^tx_1\ d^tx_2\ d^tx_3 = (det\ {}^t_0X)\ d^0x_1\ d^0x_2\ d^0x_3$$

where ${}^t_0X$ is the deformation gradient given by $({}_0\nabla\ {}^tX^T)^T$

where ${}_0\nabla^T = [\frac{\partial}{\partial {}^0x_1} \quad \frac{\partial}{\partial {}^0x_2} \quad \frac{\partial}{\partial {}^0x_3}]$ and ${}^tX^T = [\,{}^tx_1 \quad {}^tx_2 \quad {}^tx_3\,]$

Hence,

$$ {}^0\rho = {}^t\rho \;\; (det\; {}^t_0X) $$